Defence Research and Development Canada | Recherche et développement pour la défense Canada

CAN UNCLASSIFIED

DRDC | RDDC
technologysciencetechnologie

Model-to-model comparison of low-frequency acoustic models for Arctic environments

Impact of Ice

Diana McCammon
Dale Ellis
Maritime Way Scientific Ltd

Prepared by:
Maritime Way Scientific Ltd
1420 Youville Drive, Unit 5A
Ottawa ON K1C 7B3

Contractor Document Number: 13-027.11
PSPC Contract Number: W7707-145690 Call-up # 11
Technical Authority: Sean Pecknold, DRDC – Atlantic Research Centre
Contractor's date of publication: June 2017

Defence Research and Development Canada
Contract Report
DRDC-RDDC-2018-C079
April 2018

Canada

IMPORTANT INFORMATIVE STATEMENTS

Maritime Way Scientific Ltd.
Operational Oceanography & Scientific Solutions

"Building a Window to a Transparent Ocean"

www.maritimeway.ca

Model-to-model comparison of low-frequency acoustic models for Arctic environments

Impact of Ice

Dr. Diana McCammon and Dr. Dale Ellis

Solicitation Number:

Document Information

Company Project Number 13-027.11

CTC-128-AGR

Maritime Way Scientific Ltd
1420 Youville Drive, Unit 5A
Ottawa ON K1C 7B3
T: 613-841-0505 • **E:** mtaillefer@maritimeway.ca

Maritime Way Scientific Ltd
1420 Youville Drive, Unit 5A
Ottawa ON K1C 7B3
T: 613-841-0505 • **E:** mtaillefer@maritimeway.ca

Maritime Way Scientific Ltd.
Operational Oceanography & Scientific Solutions

Executive Summary

Model–to-model comparison of low-frequency acoustic models for Arctic environments: Impact of ice

McCammon, D.F. and Ellis, D.D., June, 2017

Introduction

The ice covering the Arctic oceans represents an elastic boundary that changes sound propagation. This report examines various ways of modelling that ice using two propagation models with different mathematical approaches. The normal mode model Prolos was selected to be the benchmark because of its exact treatment of range independent propagation in shallow water. It was compared to the Gaussian beam model Bellhop because that model is favoured for Naval operational use due to its speed and range dependent capabilities. In the regions of the Barrow Strait (shallow) and Baffin Bay (deep), four different boundary conditions were tested: air-backed elastic ice with shear wave capability, air-backed fluid ice with no shear generation, ice-free water (a vacuum boundary) and rigid ice with no shear generation.

Results

Comparing the four boundary conditions used to describe ice cover, the only one that was consistently poor was the rigid assumption which was significantly lower in correlation and significantly higher in rms dB error when compared to elastic ice, and the addition of a roughness scattering loss does not improve the result. With regard to ice thickness, thin ice in shallow water shows the most deviation from ice-free water. The impact of ice thickness is diminished in deeper water.

In model-to-model comparisons, Prolos and Bellhop comparison statistics are in close agreement for all four boundary conditions tested from 30 Hz to 1000 Hz. The model differences were caused by deficiencies in the mathematics of Bellhop: lack of reflection additions to receivers near the bottom and the intrusion of caustic corrections in the Gaussian beam algorithm of Bellhop at low frequencies, both of which cause an underestimation of field strength. For frequencies above 300 Hz, the models' coherent predictions are in excellent agreement.

Significance

Firstly, current methods of modelling ice as a rigid boundary with a roughness scattering loss will not correctly predict the coherent field phasing or levels. Secondly, thin first year ice will

need more careful modelling than thick multi-year ice. Finally, the Bellhop Gaussian Beam's coherent transmission loss compares favorably with the exact normal mode solution over a wide frequency band except when the receiver is too close to the boundary or when the caustic correction cap interferes with the ray amplitude.

Martin L. Taillefer, CD, M.Sc., B.Sc.
President & Managing Director
Maritime Way Scientific Ltd

Maritime Way Scientific Ltd.
Operational Oceanography & Scientific Solutions

Title & Project Identification Page

The RFP file number	
Company name and address	Maritime Way Scientific Ltd. 1420 Youville Drive, Unit 5A Ottawa, Ontario • K1C 7B3 Phone 613.841.0505 • Fax 613.590.7231
MWS Project Number	CTC-128-AGR
Contact Persons	Mr. Martin Taillefer Phone 613-841-0505 mtaillefer@maritimeway.ca Mr. Craig Hamm Phone 613-841-0529 craig.hamm@maritimeway.ca
RFP Title:	**Model-to-model comparison of low-frequency acoustic models for Arctic environments**
Short extract	

Table of Contents

List of Figures

1 INTRODUCTION

Reliable acoustic propagation models for the Arctic are essential for understanding ambient noise, communications, and sonar performance. The Bellhop model (ref.) is a very useful tool at high frequencies, though being ray-based, its performance deteriorates at low frequencies. It has proved very useful in studying open ocean environments (some of your refs?), so it would be very useful to extend it to Arctic environments, including ice-covered ones. The ice covering the Arctic oceans represents an elastic boundary that changes sound propagation. This report examines various ways of modeling that ice using two propagation models with different mathematical approaches. The normal mode model Prolos was selected to be the benchmark because of its exact treatment of range independent propagation in shallow water. It was compared to the Gaussian beam model Bellhop because that model is favoured for Naval operational use due to its speed and range dependent capabilities.

This report is part of a Research Contract between Defence Research & Development Canada and Maritime Way Scientific Ltd. We begin with a description of the tasking, and our approach to the tasks, which was to compare the Bellhop results for an ice-covered Arctic sound speed profile with predictions from a normal mode model. The next section gives a brief description of the models, the environments and frequencies chosen for study, and adjustments necessary to ensure the models are performing calculations on the same environment. The extension of the normal mode model to handle a reflection coefficient is new, so a description of the mathematics is included in an Appendix. The next section describes the ice model, which is essentially a reflection coefficient that handles multiple layers with shear waves. In order to get a reasonable measure for the model-model differences, some statistical measures of goodness-of-fit are described. These are then used to compute the impact of ice for two environments, over a number of frequencies from 30 to 1000 Hz. Then model-to-model comparisons are made for the same boundary conditions. We conclude with a discussion of the results, and some recommendations for further work.

1.1 Tasking

This report covers tasks 6.1 and 6.2 of the contract. These tasks were:

> *6.1 Model to model comparison of low-frequency acoustic models in Arctic environment*
>
> *6.1.1 Outline required scope for performing this task. This includes recommendations on the appropriate models for comparison, one of which will be Bellhop with low-frequency extensions (beam displacement).*

6.1.2 Perform a model-model comparison for accuracy and speed of low-frequency acoustic propagation in Arctic conditions. The scope of this task will depend on the results of 6.1.1.

6.2 Scoping study considering the impact of acoustically penetrable ice.

Ice is often assumed to be perfectly rigid. In reality, the impact of acoustically penetrable ice decreases as frequency decreases, as the acoustic wavelength in the ice becomes long relative to its thickness. A brief study of the importance of penetrable solid floating ice in Arctic modeling is warranted.

1.2 Approach

The goal was to determine if Bellhop was a suitable tool for using in an ice-covered Arctic environment, by comparing it with another model, and to determine if it was useful at frequencies below the generally-assumed limit of 20 or so water depths. Not many Arctic models are available (Etter, 2013). The approach taken was to add beam displacement to Bellhop and compare with the "exact" solution from a normal mode problem – an approach that had been used earlier for open-ocean environments (McCammon & Ellis, 2015).

The approach to these tasks was as follows:

Task 6.1 Objectives

a) Using Bellhop and Prolos as the two models best suited for this task, this report will describe the adjustments required to bring the two models into agreement and document any model shortcomings such as physics that may not be modelled correctly.
b) The report will describe the elastic ice reflection model to be employed by the two propagation models and how that reflection model is fitted into Prolos.
c) The report will mention the difference in behaviour between using a roughness loss model and using shear wave losses.
d) The divergence of Bellhop from Prolos will be demonstrated in frequency, ice thickness, shear wave losses, source/receiver depth, etc.

Task 6.2 Objectives:

a) This report will try to show how model limitations affect the results by contrasting various boundary conditions with penetrable layered ice including shear wave propagation.
b) This report will try to determine when ice penetration is important with respect to frequency and ice thickness as a function of range. It will consider when simple roughness might mimic penetration.

2 PROPAGATION LOSS MODELS

2.1 Bellhop

For this study, the web version Bellhop2D from the (8 August 2016 release) (Ocean Acoustics Library, last accessioned June 1, 2017) is used. It was subsequently adapted to this task by inserting the choice of an outside elastic reflection model (McCammon & McDaniel, 1985) for surface reflections from ice. The model was exercised using the Gaussian Beam algorithm ('B') with a fluid-halfspace sediment ('A'). The angle fan was ±25° and the number of rays was 4001. The beam displacement option was used for both surface and bottom ('S'). The SSP was linearly interpolated and no additional volume attenuation (Thorpe) was added.

2.2 Prolos

The normal mode calculations were performed with a modified version of Prolos (Ellis, 1985). The Prolos model is applicable to an environment having fluid layers, with a pressure release boundary at the surface and a halfspace at the bottom. It is possible to extend the normal mode formulation to handle elastic layers (Hughes, Ellis, Chapman, & Staal, 1990), but the procedure is more complicated and subject to numerical issues. The approach taken here was to adapt Prolos to handle an arbitrary reflection coefficient at the ocean surface. The mode boundary condition can be obtained from the phase of the reflection coefficient, and the mode attenuation coefficient obtained from the reflection loss and cycle distance (Tindle & Weston, 1980). Details of the procedure are included in the Appendix A.

Our calculations used the identical reflection coefficient code as Bellhop – the elastic-layer ice reflection coefficient of (McCammon & McDaniel, 1985). Thus, errors from potential differences in the treatment of shear waves in the ice are avoided.

The Prolos model uses a staircase of isospeed layers, interpolated to approximate the input sound speed profile. For the calculations here, 1000 layers were used. The transmission loss (TL) is calculated using both a coherent and incoherent summation of modes, the latter producing a smooth monotonically-decreasing average as a function of range.

2.3 Comparison environments

Ice study parameters

Frequencies: 30, 50, 100, 300, 500, 800, 1000 Hz
TL: Range to 20 km in steps of 10 m
SSP linear gradient: 0 m – 1440 m/s, 250 m – 1452.5 m/s, 2200 m – 1488.0 m/s
Water density: 1.028 g/cc
Water depths: Barrow Strait: 250 m; Baffin Bay: 2200 m

Bathymetry: flat
Source depths: Barrow Strait: 100 m and 240 m; Baffin Bay: 100 m and 2050 m
Receiver depth: Barrow Strait: 100 m and Baffin Bay: 2050 m
Bottom composition; silty sand halfspace: density = 1.8 g/cc, speed = 1568.7 m/s, attenuation = 0.44 dB/mkHz
Air backing of ice: air density = 0.001223 g/cc, air speed = 332 m/s
Water backing of ice: water density = 1 .028 g/cc, compressional speed = 1440 m/s
Ice properties: density = 0.91 g/cc, compressional speed = 3600 m/s, compressional attenuation = 0.068 dB/mkHz, frequency exponent = 1; shear speed = 1800 m/s, shear attenuation = 0.408 dB/mkHz, frequency exponent = 1
Ice thickness = 0 to 6 m

The SSP was linearly interpolated and no additional volume attenuation (Thorpe) was added.

2.4 Adjustments to bring the two models into agreement

2.4.1 Trapped modes

The Prolos normal mode formulation includes only the trapped modes, so contributions to the acoustic field above the critical angle are neglected. It is possible to include a false bottom, and allow steeper propagation angles, but generally that is a bit tricky. The easier way to do our model-model comparisons is simply to restrict Bellhop to angles below the critical angle. If angles above the critical angle are needed, e.g., at short ranges in deep water, then Bellhop can be first validated at the low angles, and later extended to include the higher angles.

2.4.2 Harder sediment

The first test run was for 300 Hz to establish a point of agreement. Initially with the source and receiver 10 m above the bottom at 240 m, and using a vacuum surface boundary condition and a simple fluid halfspace for the sediment with an estimate for silty sand sediment in which the sound speed ratio was unity and the density 1.17, we found very poor agreement. The low basement sound speed made it necessary to define a false sub-bottom layer to get steeper angles in Prolos, and that resulted in its TL levels being considerably above Bellhop. The low basement sound speed was physically unrealistic so it was decided to choose a faster and harder sediment with compressional speed 1568.7 m/s, density 1.8 g/cc and attenuation 0.44 dB/mkHz. Following that adjustment, the two model results were in excellent agreement in phasing, however, as shown in Figure 1 the models were still in poor agreement in level, with Bellhop being consistently low.

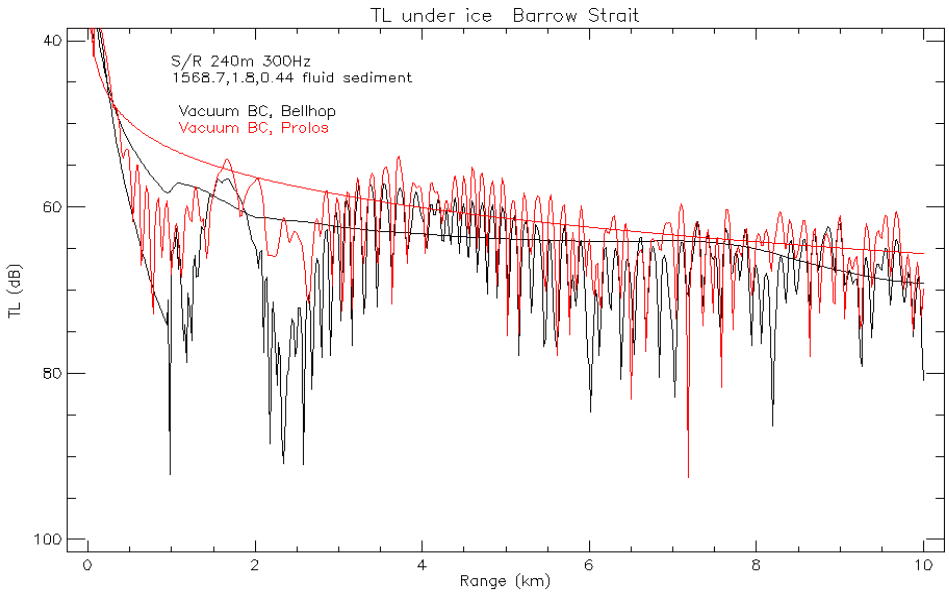

Figure 1. Harder bottom: 300 Hz, s/r 240 m, Prolos (red), Bellhop Gaussian function (black).

Note also that the incoherent results are very different, with the incoherent mode summation in Prolos giving a smooth monotonically decreasing curve while the Bellhop result shows more structure. This expected since they are computed in fundamentally different ways. However, the normal mode incoherent summation is a well-defined range average of the intensity, so it will be chosen for all normalizations for consistency.

The level differences are explored in section 2.4.4.

2.4.3 Receiver away from the bottom

The Bellhop users guide (Porter, 2010) suggests not using the model for receivers near the boundaries, because the ray method does not account for secondary ensonification from the boundary. The addition of image sources (green) shown in Figure 2 (top) does improve the Bellhop Gaussian Beam levels, but not enough, and since the image sources are not included in the web version of Bellhop, it was decided not to employ them. In Figure 2 (bottom) the Bellhop GeoHat algorithm (Porter, 2010) was tested and found to reproduce the correct level but it showed instabilities. This is discussed further in Section 2.4.4.

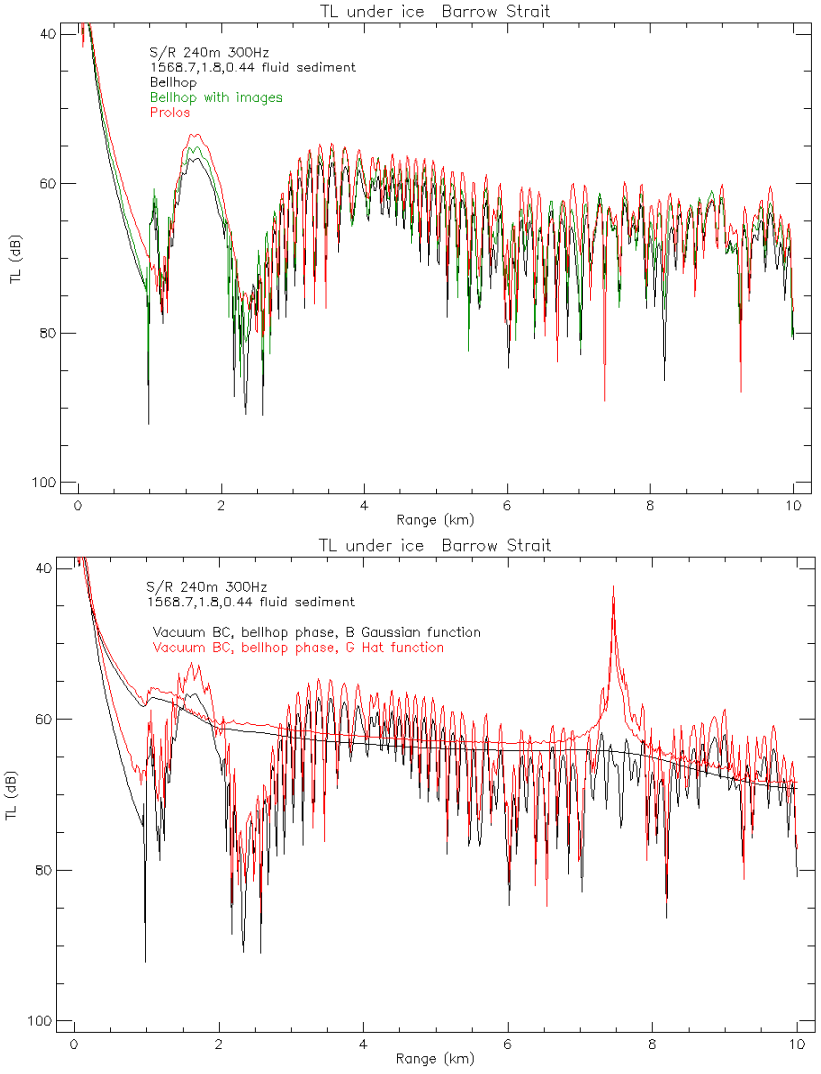

Figure 2. Top- Image sources: Prolos (red), Bellhop (black) and Bellhop with images (green). The image sources do bring up the level, but not sufficiently. Bottom- Bellhop GeoHat function (red) brings the level up but shows instability.

Finally, it was decided to move the receiver away from the bottom boundary, and with this adjustment, the two models, Prolos and Bellhop Gaussian Beam, show excellent agreement, both in level and phase, as shown in Figure 3.

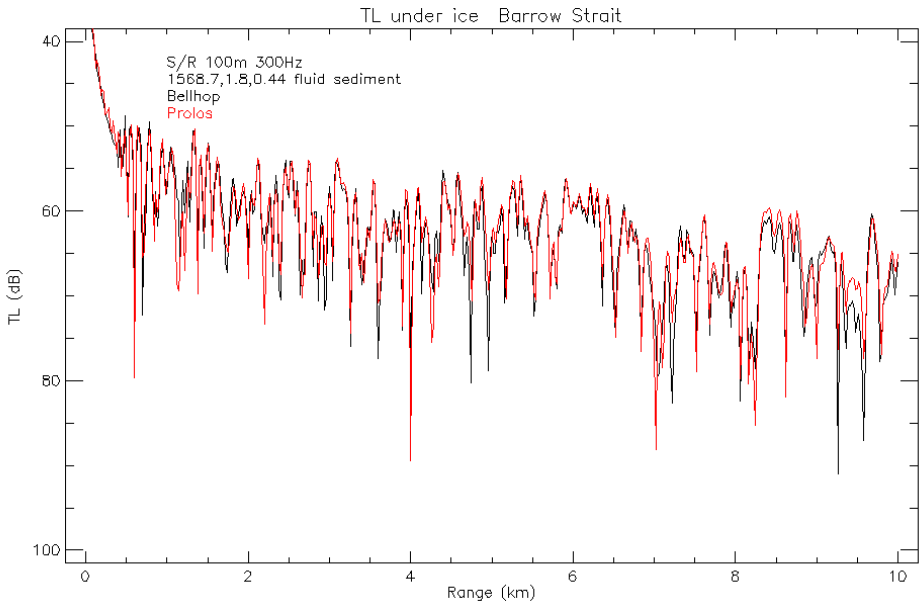

Figure 3. Higher receiver: s/r 100 m, 300 Hz, Prolos (red), Bellhop (black).

2.4.4 Bellhop cutoff and GeoHat algorithm

Next, the frequency was lowered to 50 Hz, and the two models were again compared. It was found that the Bellhop predictions were consistently lower than Prolos. To try to find the additional attenuation Bellhop seemed to have, the boundary conditions were further simplified to remove all outside attenuation. The bottom was modelled as rigid, the top as a vacuum and no volume attenuation was used. Figure 4 (top) shows the transmission loss versus range for a source depth of 240 m and a receiver depth of 100 m. Prolos is plotted in red and Bellhop with the Gaussian algorithm in black. While the phasing is good, the level of Bellhop is consistently low. Figure 4 (bottom) shows the same scenario using Bellhop's GeoHat algorithm and now the levels between Prolos and Bellhop are much closer.

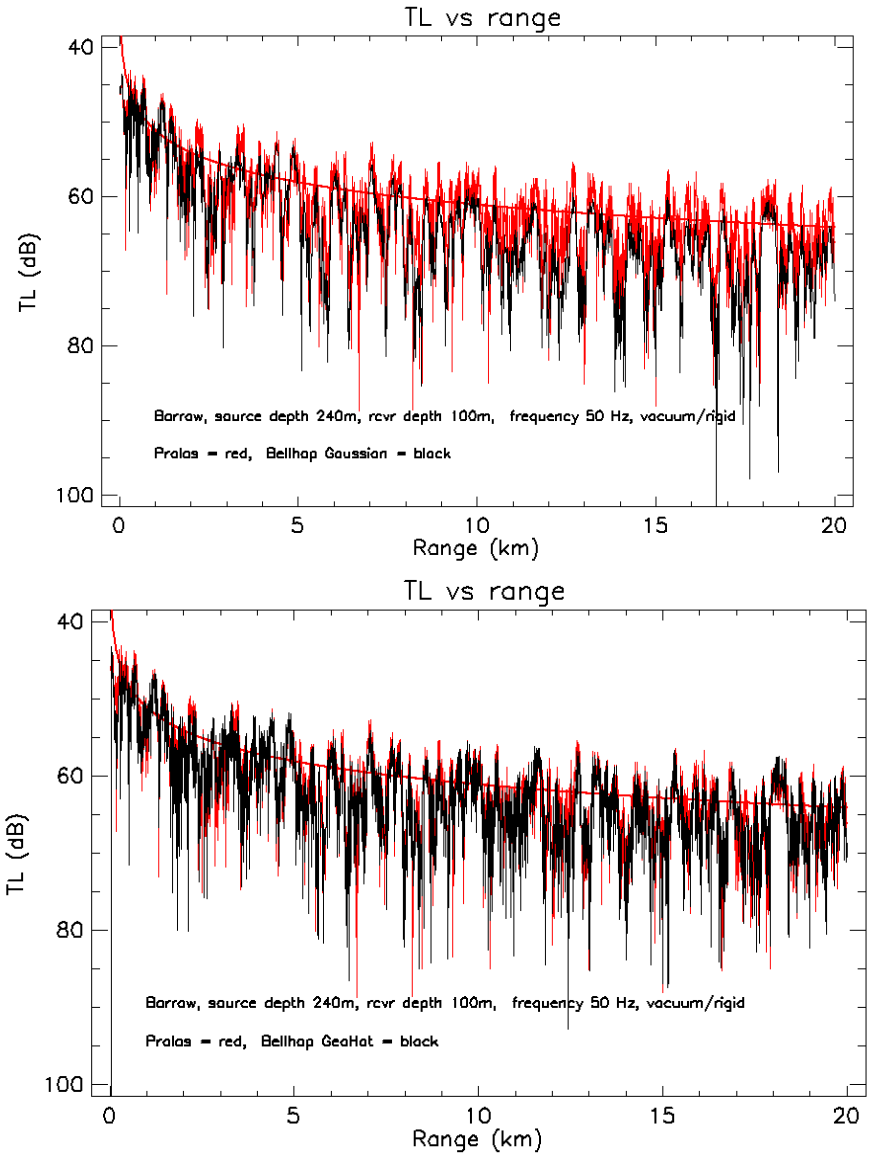

Figure 4. Two Bellhop functions: 50 Hz, s/r 240/100 m vacuum/rigid. Top: Prolos (red), Bellhop Gaussian (black). Bottom: Prolos (red), Bellhop GeoHat (black).

The difference in the two algorithms lies partially in the definition of their spatial weighting functions. (Baxley, Bucker, & Porter, ECUA 2000), (Jensen, Kuperman, Porter, & Schmidt, 2011). In the Gaussian algorithm, the weight can be written as $W_{Gaussian} = \exp\left[-0.5\left(\frac{n}{\sigma}\right)^2\right]/\sigma$, whereas in the GeoHat algorithm $W_{Hat} = (\sigma - n)/\sigma$. In these equations, n is the normal distance from the receiver's position to the ray's position. In the Gaussian algorithm, the value of σ is limited to the larger of itself or πλ, to smooth the calculation over regions where σ is very small, which will occur in the neighborhood of a ray turning point where sinθ is small. It can be

thought of as similar to the traditional caustic limit for ray theory, although the trigger is not the crossing of two rays. Thus, at low frequencies (large wavelengths), this limit will often be invoked and the level of Bellhop in those rays will be kept low. In Figure 5 (top), this limitation of σ has been removed from the Gaussian algorithm, and the levels of Bellhop (black) rise to match Prolos (red). While this programming change has enabled the levels to agree in this case, it will cause problems in other cases, as shown in Figure 5 (bottom) where it is tested at 300 Hz and several spikes appear similar to the GeoHat function, and therefore removing the limitation of σ is not recommended.

However, we can now expect and explain why the low frequency cases might exhibit a low Bellhop level, and it will have nothing to do with the boundary conditions of the scenario or the receiver's proximity to the boundary. It will be due to the wavelength limitation used for caustic corrections.

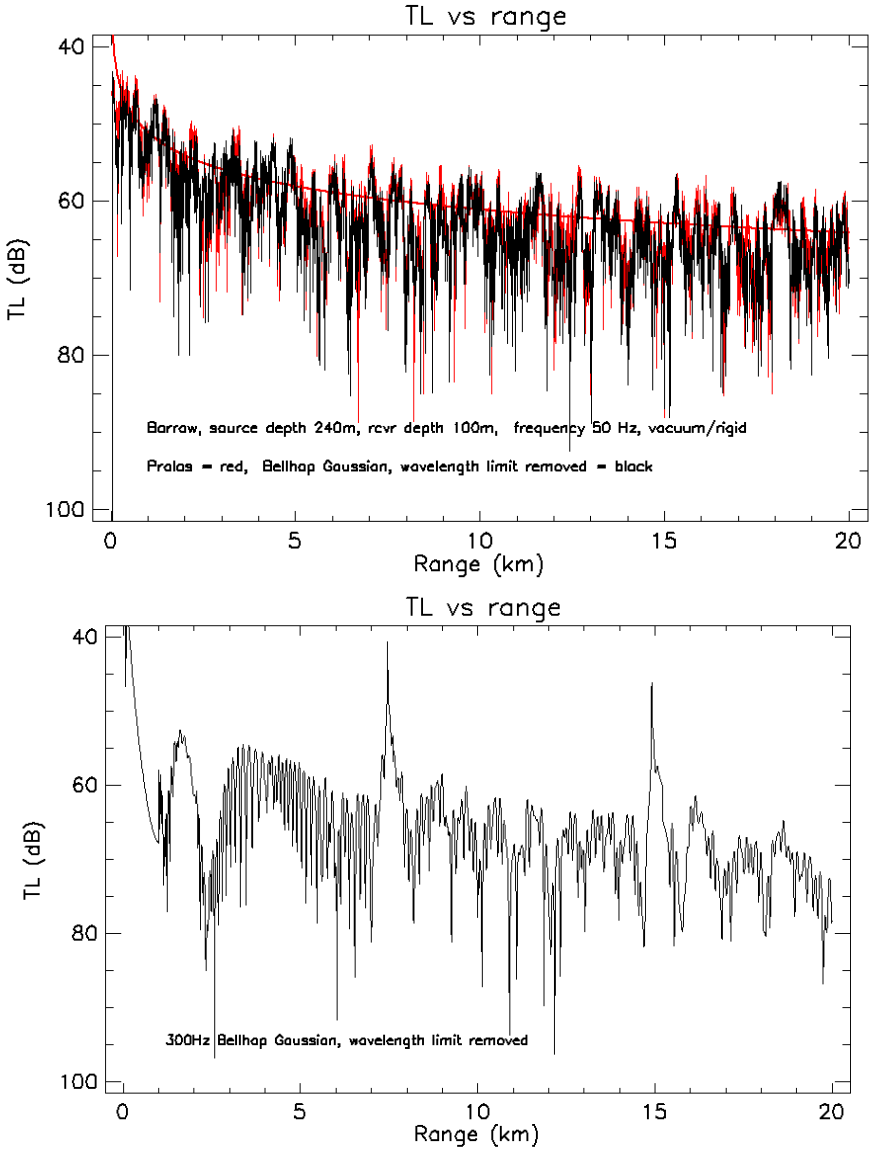

Figure 5. Bellhop Gaussian wavelength limit removed. Top: 50 Hz, Prolos (red) vs Bellhop (black). Bottom: 300 Hz Bellhop.

2.5 Tests over various boundary conditions

In Figure 6 the transmission loss vs range results from Bellhop, Gaussian algorithm, are plotted for different boundary conditions, including (on the top), 3 m elastic ice, 3 m fluid ice air backed, a fluid halfspace and a vacuum and (on the bottom), 3 m elastic ice and rigid boundary conditions. The source and receiver were at 100 m and the frequency was 300 Hz. Changing the boundary conditions in the top plot results in small shifts in phasing and level that become more

noticeable farther downrange. However, there seems to be little difference between them. Contrast that with the bottom plot where the rigid boundary condition (green) changes the comparison a great deal in both level and phase.

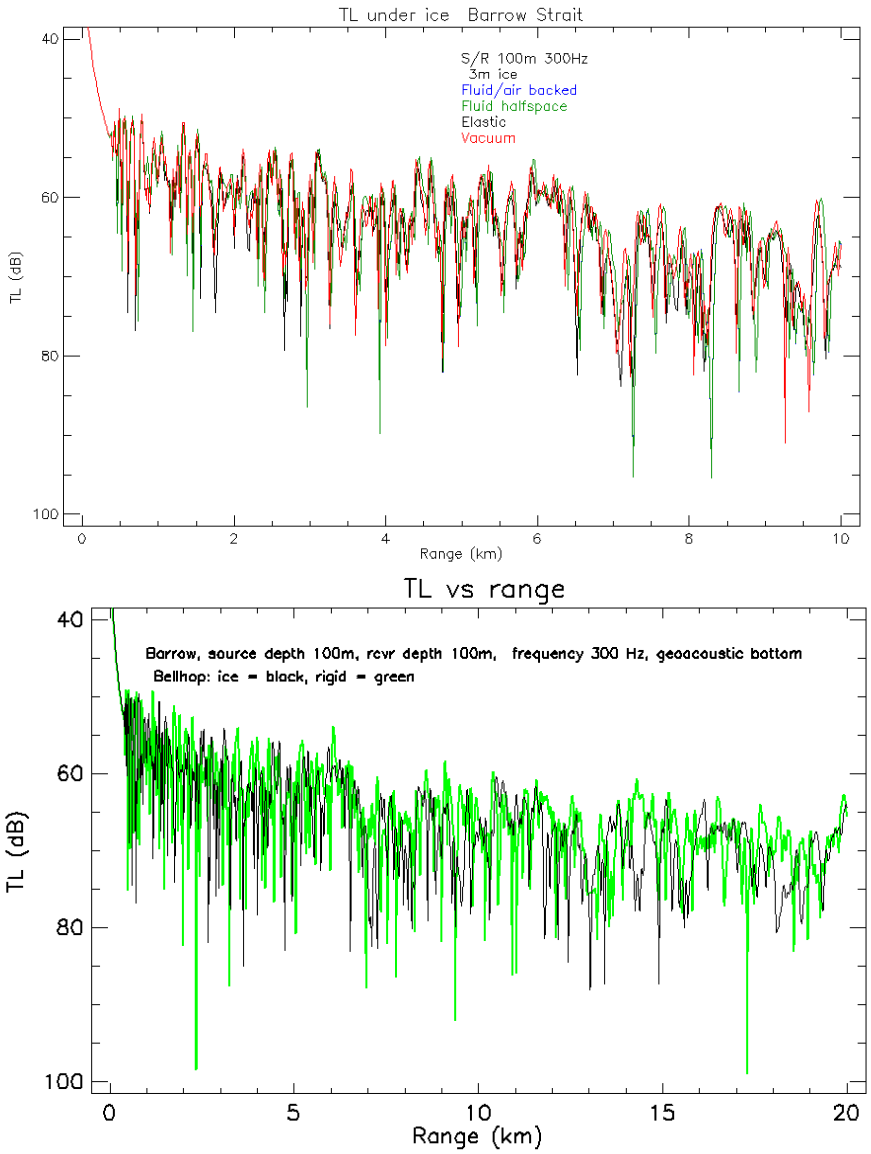

Figure 6. Boundary conditions: Bellhop TL at 300 Hz, s/r 100 m. Top: ice with shear, fluid air backed, fluid halfspace, and vacuum. Bottom: ice with shear and rigid.

3 ICE MODEL

3.1 Mathematics of Ice Model

The model for ice reflectivity is taken from (McCammon & McDaniel, 1985). The model for plane wave reflection solves a set of simultaneous equations in the compressional and shear displacement potentials and their normal derivatives.

Two typos in the paper were discovered in the model testing. First, in that paper's Eqn.16, a sign error was found in the definition of V. It should read $V = (-2/k_{sN}^2)H_2 - (1 - 2k_n^2/k_{sN}^2)H_3$. Second, in the definition of the first element in the D matrix in Eqn. 10, a density factor was omitted. It should read $D(1,1) = \frac{\rho_1}{\rho_w}\ (1 - \frac{2\,\mu_1 k_n^2}{\rho_1 \omega^2})$.

Figure 7 demonstrates the reflection coefficients vs incident angle at 2 kHz with 0.8 m ice with the above corrections in the ice model. These are compared to those computed by the program BOUNCE created by Dr. Michael Porter, available from the web on the Ocean Acoustic Library website (Ocean Acoustics Library, last accessioned June 1, 2017) shown in blue for air backing, and compared to the Safari model supplied by Dr. Gary Brooke shown in red for water backing.

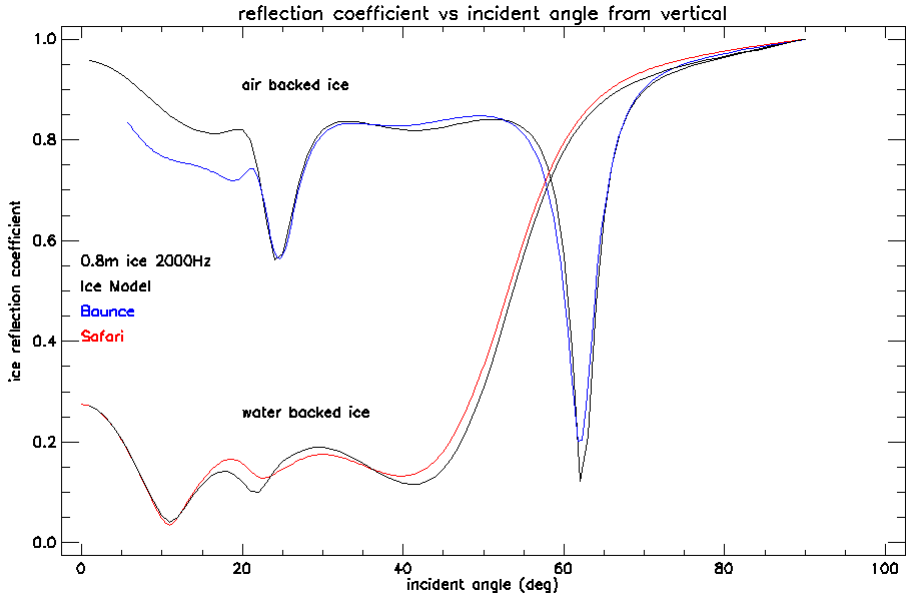

Figure 7. Two examples of ice model (black) compared to BOUNCE (blue) and SAFARI (red) with air and water backing.

The phase produced by this ice model appears to be rotated by 180°, in comparison with the value known to be correct for a fluid at 0° grazing. Therefore, the phase φ is produced from the

complex reflection coefficient $\Re$ by the trigonometric relation using a quadrant change in the denominator:

$$\varphi = \arctan\left(\frac{i\text{mag}(\Re)}{\text{real}(-\Re)}\right).$$

Also, note that the phases used in surface and bottom reflections in Prolos and Bellhop differ by a minus sign. By convention, Bellhop uses positive phases while Prolos uses negative phases, so these differences were carefully noted and programmed in each of the models.

3.2 Limitations of Ice Model

The following is a list of perceived limitations of the ice model and/or its implementation:

1. This ice reflection model contains no scattering losses due to roughness. Bellhop permits the definition of a range dependent altimetry similar to its range dependent bathymetry, which can be used to portray an ice keel field. However, this study was not addressing the impact of the range dependence of the ice roughness, but instead it was to concentrate on the effects of modelling ice as an elastic media versus either a rigid or a fluid boundary. And the model-to-model comparisons were between Bellhop, a ray model, and Prolos, a normal mode model with adiabatic range dependence. Therefore, in the implementation of this ice model in Bellhop, the model's inputs of ice properties and thickness were not made range dependent and the under-ice topography was assumed flat.
2. While the ice model can handle layers of ice of differing properties, they must all be elastic meaning it cannot predict the effects of occluded seawater pockets.
3. The model seems to be unstable in thick ice. Figure 8 (top) demonstrates a lot of low angle instability occurring in 10 m ice thickness at 600 Hz (black) which is an h/λ of 1.6. There is some slight instability in the 6 m ice at 600 Hz (blue) (h/λ of 1.0) between 60° and 70° grazing. The majority of our study will be conducted for 1 m and 3 m ice up to 1000 Hz for which the h/λ is always less than unity and the reflection coefficient curves appear stable Figure 8 (bottom).

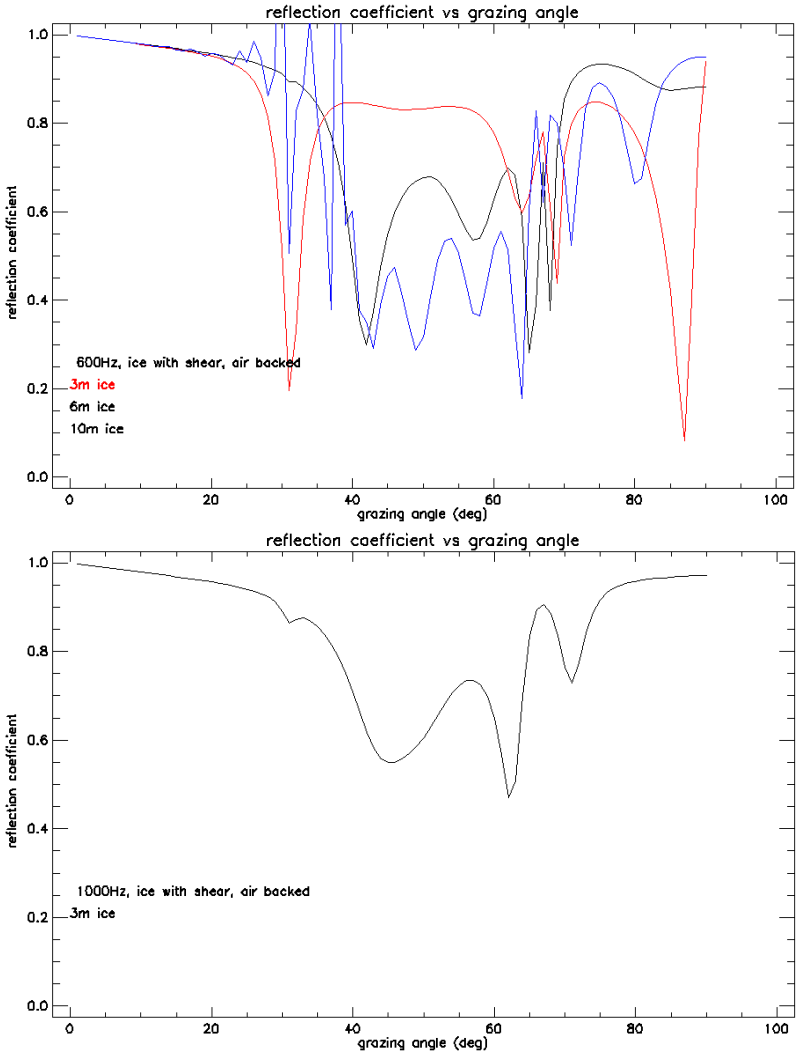

Figure 8. Ice reflection coefficient. Top: Ice of various thicknesses at 600 Hz. At the important low grazing angles, 3 m (red) and 6 m (black) are relatively stable but 10 m (blue) fails at the low grazing angles and oscillates unnaturally from 20° to 40°. Bottom: reflection coefficient for 3 m thick ice at 1000 Hz.

3.3 Example of Ice Model Reflection Coefficients

The ice model is capable of treating the entire ice thickness as a fluid using a simple Rayleigh two-layer reflection model. Figure 9 shows an example of reflection coefficients vs grazing angle for three cases at 300 Hz. In Figure 9, (top and bottom), the black curve is 3 m of ice with shear, air backed. The red curve is 3 m of fluid ice with no shear, air backed, and the blue curve is the reflection coefficient from a fluid halfspace. It can be seen in the top plot of this figure that ignoring shear waves will neglect the losses at the lower grazing angles that would be important for long range propagation. Above 66°, the two fluid treatments diverge, but this

would only affect short range propagation. Rigid surface boundary conditions would produce a unity reflection coefficient and zero phase at all angles.

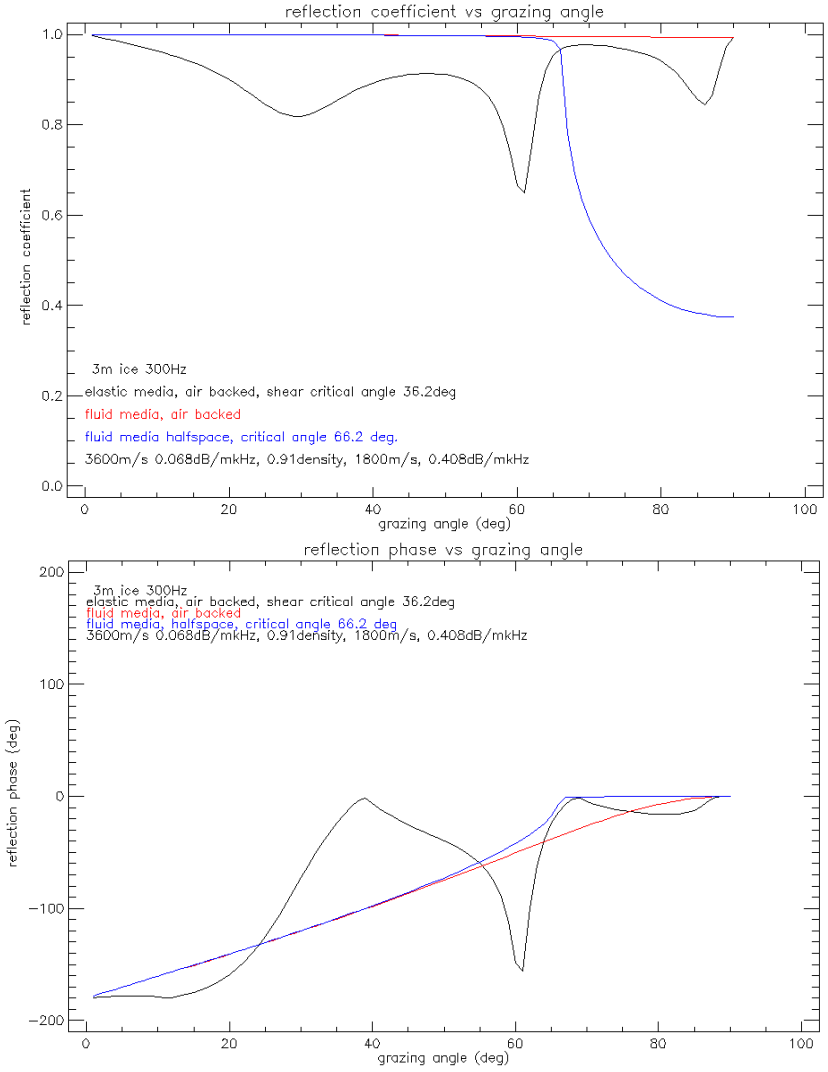

Figure 9. Reflection coefficient and phase for 3 m of ice at 300 Hz, a comparison of different treatments of the boundary.

3.4 Roughness Models vs Shear Wave Models

In the Kirchhoff theory of roughness scattering in (Ogilvy, 1991), the total scattered field will be the sum of the coherent field and the diffuse field, with the diffuse field dominating for large roughness. The coherent field in the specular direction is decreased by the factor $\exp(-g) = \exp[-(2k\,\sigma\,\sin\theta)^2]$, in which the Rayleigh Roughness parameter is $(k\,\sigma\,\sin\theta)$, σ is the rms surface deviation from smooth and θ is the grazing angle. This amplitude reduction can be included (and Prolos has it already), but it does not cause any phase change in the field, whereas

a fluid or elastic treatment of the penetrable ice media does cause phase changes. Figure 10 shows transmission loss from Bellhop at 300 Hz for an ice surface with the reflection phase set to zero (red) versus an ice surface with the proper phase shift (black). This shows that using the simple loss term will not correctly provide the transmission loss phasing that the ice would create.

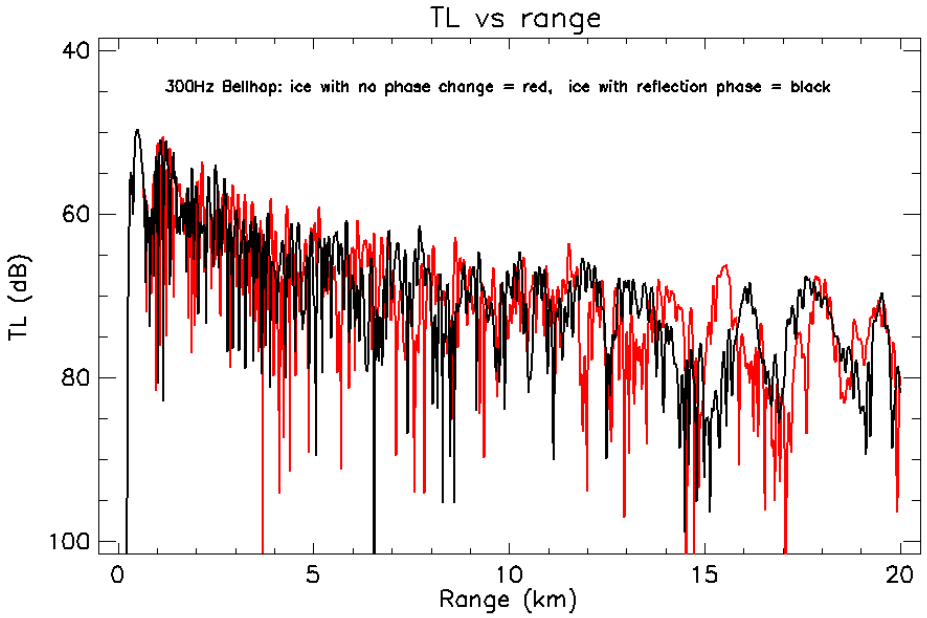

Figure 10. Ice with loss but no phase change (red) vs ice with correct reflection phase changes (black). Lack of phase change throws the correlation of the curve off.

4 STATISTICS OF TL CURVES USED TO HIGHLIGHT DIFFERENCES

The following statistical measures of goodness-of-fit are computed for each model to compare the differences in ice vs fluid vs vacuum boundary conditions. They are also computed in model-to-model comparisons for each boundary condition. By these measures we draw our conclusions:

- Impact on ice on both models leading to generalizations about the validity of simplified boundary conditions.
- Validity of Bellhop by comparison to Prolos under all tested boundary conditions and frequencies.

4.1 Correlation and lag

To establish the phase relationships between the TL from the two cases being compared he first statistic that seems important is to perform a correlation. IDL software is used to produce this statistic.

1. Convert the dB transmission losses into intensity by $= 10^{-TL/10}$.
2. Detrend the intensities by multiplication by the range $I_d = I\, r$.
3. Cross correlate the two detrended arrays using the IDL function C_CORRELATE (A_1, A_2, lag) where lag is a vector from –(N-1) to +(N-1). The lag identifies the position of the best correlation between the two arrays.
4. Shift the second array to line up with the first using the location of the maximum correlation and the IDL function SHIFT.
5. Plot the correlation and record its maximum value and lag.

Figure 11 displays an example of cross correlation between Bellhop and Prolos for the 300 Hz case with ice cover for two source depths, 100 m (black) and 240 m (red) in the Barrow Strait.

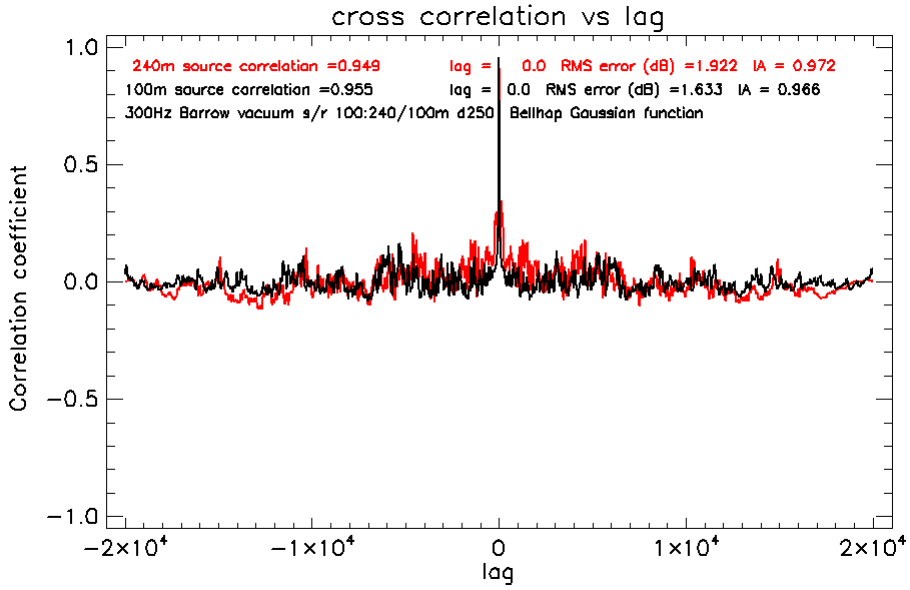

Figure 11. Example correlations between Prolos and Bellhop at 300 Hz over vacuum BC for two source depths. The lag on the horizontal axis is the number of sample points from the center of the array.

4.2 Index of agreement

The Index of agreement, IA, is defined as the error referred to the potential error, with perfect fit being unity. ((Statistics, last accessioned June 1, 2017) eqn 9, and note mistake in MATLAB code below definition). The normalization is on both data sets so it minimizes bias. And it is constructed from intensity so it still favours the high intensity regions rather than the nulls. For this calculation, the first 1 km of data are skipped so that the short range high intensity values won't bias the result. The equation for the IA between two sets of data, *x1* and *x2* is:

$$IA = 1 - \frac{< (x1 - x2)^2 >}{< (\ |x1 - < x1 >| + |x2 - < x2 >| \ )^2 >}$$

In the Figure 11 above, the IA for the vacuum comparison between Bellhop and Prolos at 300 Hz is 0.966 for the 100 m source and 0.972 for the 240 m source, which is an interesting slight reversal of goodness-of-fit from the correlations which gave the better fit to the 100 m source.

4.3 Rms dB error

After experimentation with the rms error, it was decided to proceed using the dB values of the TL. It is recognized that that will accentuate the nulls where the loss is higher and where the two cases being examined are most often likely to disagree, however, by capping the loss with a suitable threshold to remove the deeper nulls, the resulting dB error seems visually reasonable. The alternative is to compute the rms error in intensity space and then convert to dB by some suitable normalization. This will accentuate the peaks of the intensity, but it produces a rather

large error that seems unreasonable on visual inspection of the two curves. Therefore, the steps taken to generate the rms dB error are:

1. Convert the detrended and lag shifted arrays used for the correlation calculation into dB by $TL = -10\,log_{10}(I_d)$.
2. Skip the first 1 km of data to produce arrays with relatively uniform excursions.
3. Set the dB cap at the incoherent Prolos level + 10 dB.
4. Skip all ranges where either of the two arrays exceeds the cap.
5. Sum the squared differences between the two arrays over range, and count the number of terms.
6. Form the mean of the squares by division by the number of terms, then take the square root.

Figure 12 shows an example of the detrended and shifted arrays from the comparison between Bellhop and Prolos at 300 Hz over ice. The lower curves are for the 100-m source, and the upper curves are for the 240-m source. Prolos is in red, Bellhop is in blue and black. The smooth red line on both is the Prolos incoherent detrended value + 10 dB, which is the high loss cap. The resulting rms error is 1.633 dB for the 100-m source and 1.922 dB for the 240 m source.

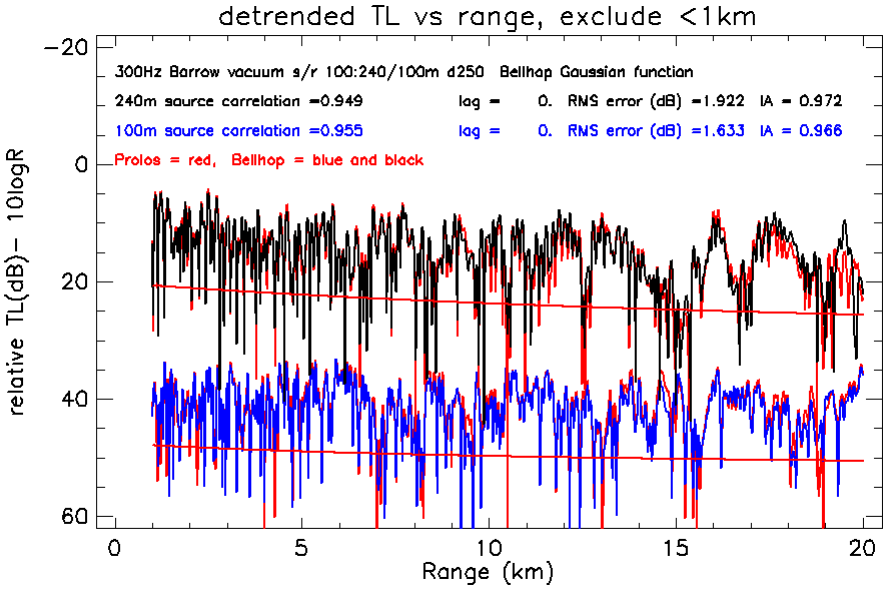

Figure 12. Detrended and shifted arrays for 100 m (lower) and 240 m (upper) source depths at 300 Hz. Rms null cutoff, shown by the smooth red line, is the detrended incoherent Prolos + 10 dB.

4.4 Other statistics

There are numerous methods for comparing the differences between models (Willmott, et al., 1985)

Several other statistical measures were examined. They included:
the mean error also called the bias: $ME = < x_1 - x_2 > = < x_1 > - < x_2 >$;
the mean absolute error $MAE = < |x_1 - x_2| >$;
and the standard deviation of residuals: $SDR = \sqrt{(< [(x_1 - < x_1 >) - (x_2 - < x_2 >)]^2 >)}$.
It was felt that these statistics did not bring any new insight beyond that gained from the previous 3 statistics, therefore they were not computed.

5 IMPACT OF ICE IN EACH OF THE MODELS

In this section, each model's output is independently compared for various boundary conditions, that is, each comparison is between the same model for different boundaries. Both models' results are shown on the graphs. The model-to-model statistics are following in the next section.

5.1 Barrow Strait

The Barrow Strait region chosen for this study featured a flat 250 m depth with a two point sound speed profile [0 m,1440 m/s] to [250 m,1452.5 m/s] that produces a positive upward refracting gradient of 0.05 m/s/m. The receiver was placed at 240 m depth.

5.1.1 Same model with different boundary conditions

Correlation and IA vs frequency, same model, different BC

Figure 13 shows the correlation as a function of frequency from 30 Hz to 1000 Hz between transmission loss from the same models under 3 m of ice with shear versus ice without shear (fluid ice) (top), a vacuum (middle) and a rigid BC (bottom) for a source depth of 100 m (solid line) and 240 m (dashed line). The statistics from both models are plotted, with Prolos in red and Bellhop in black.

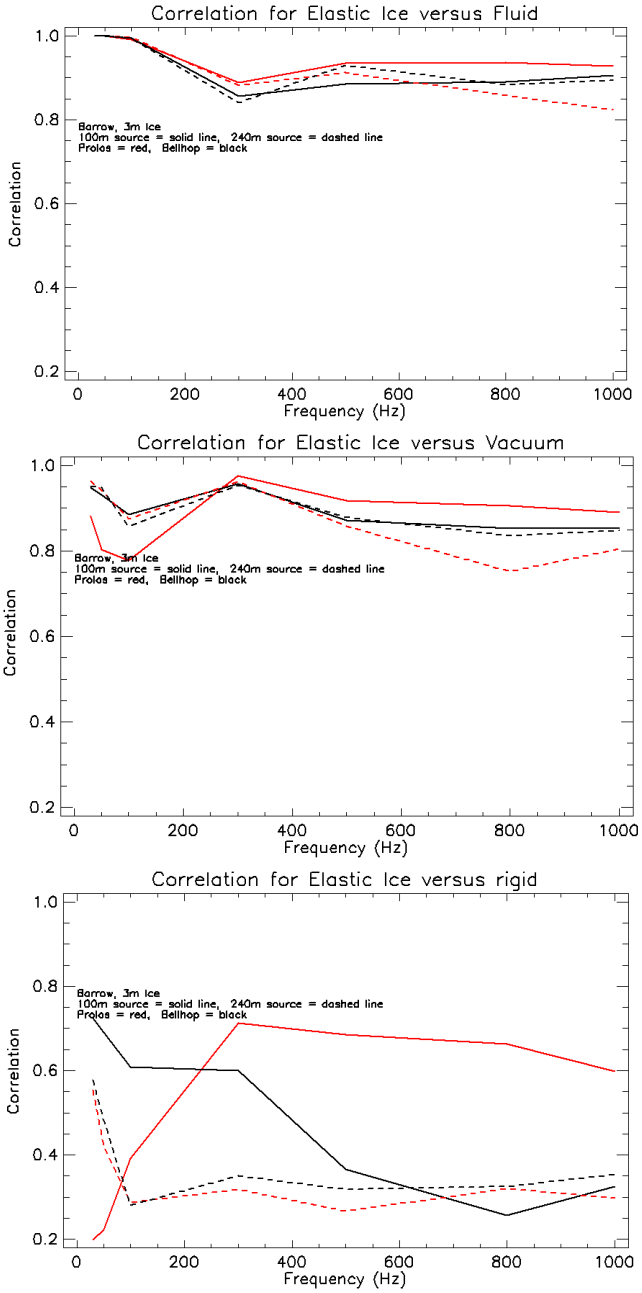

Figure 13. Impact of 3 m ice in Barrow Strait: Correlations vs frequency for sources at 100 m (solid) and 240 m (dashed), Prolos (red) and Bellhop (black). Top: correlation between elastic and fluid ice. Middle: correlation between elastic ice and vacuum. Bottom: correlation between elastic ice and a rigid boundary condition.

Figure 14 shows the index of agreement vs frequency for ice vs fluid (top), ice vs vacuum (middle), and for ice vs rigid (bottom) for each model at two source depths. The statistics from both models are plotted, with Prolos in red and Bellhop in black.

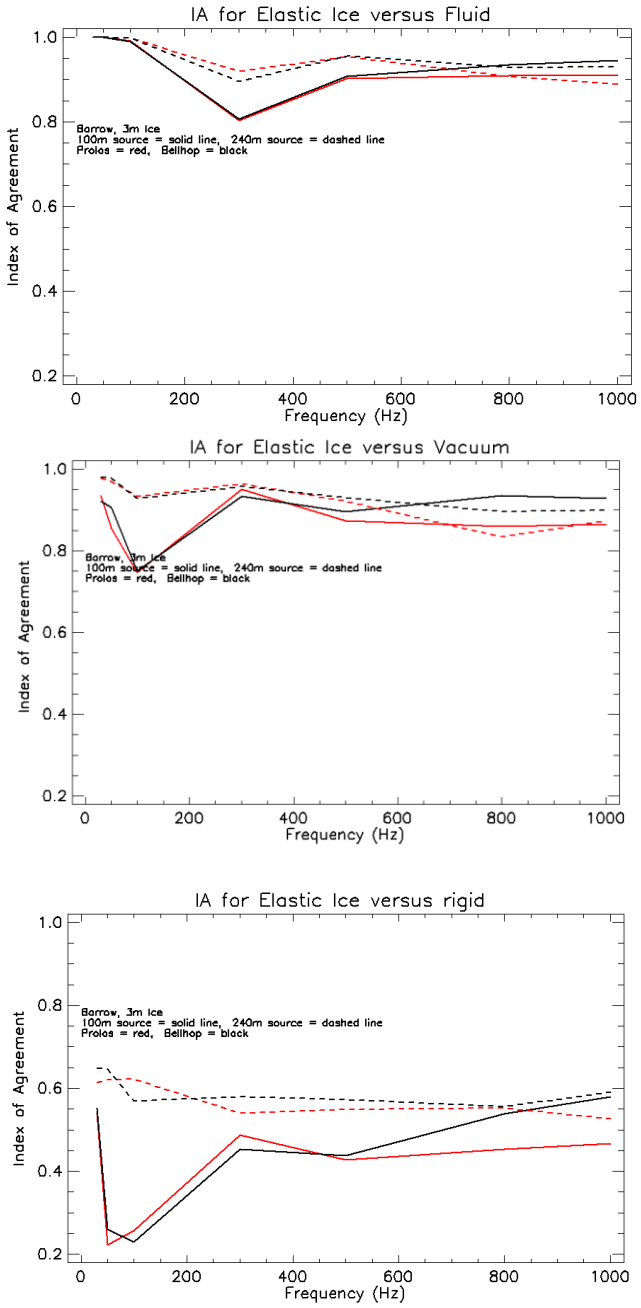

Figure 14. Impact of 3 m ice in Barrow Strait: Index of Agreement vs frequency for sources at at 100 m (solid) and 240 m (dashed), Prolos (red) and Bellhop (black). Top: IA between elastic and fluid ice. Middle: IA between elastic ice and vacuum, Bottom: IA between elastic ice and a rigid boundary condition.

Rms dB error vs frequency, same model, different BC

Figure 15 shows the rms dB error vs frequency for ice vs fluid (top), ice vs vacuum (middle) and ice vs a rigid boundary condition (bottom) at two source depths for each model. Prolos is shown in red and Bellhop in black.

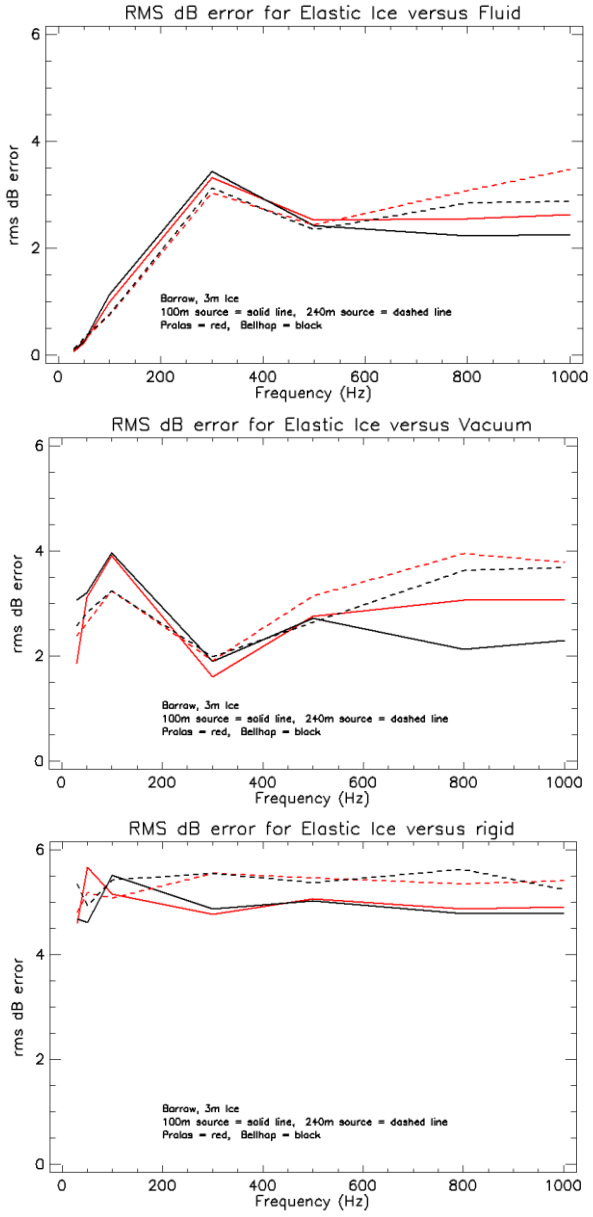

Figure 15. Impact of3 m ice in Barrow Strait: Rms dB error vs frequency for sources at 100 m (solid) and 240 m (dashed), Prolos (red) and Bellhop (black). Top: Rms error between elastic and fluid ice. Middle: Rms error between elastic ice and vacuum, Bottom: Rms error between elastic ice and a rigid boundary condition.

Observations from these statistics

The statistics in this section are comparisons of the ice vs fluid, ice vs vacuum, and ice vs rigid boundary conditions using the same model in the Barrow Strait. Both model statistics are shown, Bellhop is black and Prolos is red. Source depths are shown as solid or dashed lines. The following observations are made:

Low frequencies

- Fluid ice (no shear): Both the correlation and the index of agreement statistical measures are basically showing the same trends and both have very high values at lower frequencies for the fluid case, which leads to the conclusion that at frequencies below 100 Hz, the elastic nature of the 3 m of ice is not important and it can be treated as a fluid. The rms error also supports this conclusion, falling to a very low value under 1 dB below 100 Hz.
- Vacuum (ice-free): In the comparison of ice vs vacuum, the statistics are all somewhat poorer, correlations lower, errors higher, than the fluid case, which leads to the conclusion that the high-speed interface should not be ignored, even if it is not necessary to use an elastic treatment.
- Rigid (no penetration, no phase shift): In the comparison of ice vs rigid, the statistics are very poor. Correlations and IA values are much lower and the rms errors are several dB higher than either of the other two cases. The lack of phase change in a rigid boundary condition is responsible for this poor agreement.

High frequencies

- Correlation and IA level off above 500 Hz to a fairly high level of about 0.9 in the fluid case. This seems to indicate that the phase differences between solid and fluid treatments is not important at low angles of propagation.
- There is a frequency specific shear wave related phenomena that occurs about 300 Hz and affects both source depths.
- There is an inversion at 300 Hz between the 100-m source and the 240-m source, where the statistics reverse the importance between fluid and vacuum.
- The rigid boundary condition is in very poor agreement with elastic ice in all statistics and appears to exhibit about the same rms error at all frequencies and source depths.

5.1.2 Ice thickness effects

The importance of the ice thickness in the Barrow Strait was studied using Bellhop, Gaussian algorithm. Frequencies from 30 Hz to 1000 Hz were input for ice thicknesses varying from 0 to 6 m. Both source depths of 100 m and 240 m were tested with the receiver at 100 m. The statistics are plotted in Figure 16 for all frequencies and source depths, and those that show unusual behavior are labeled.

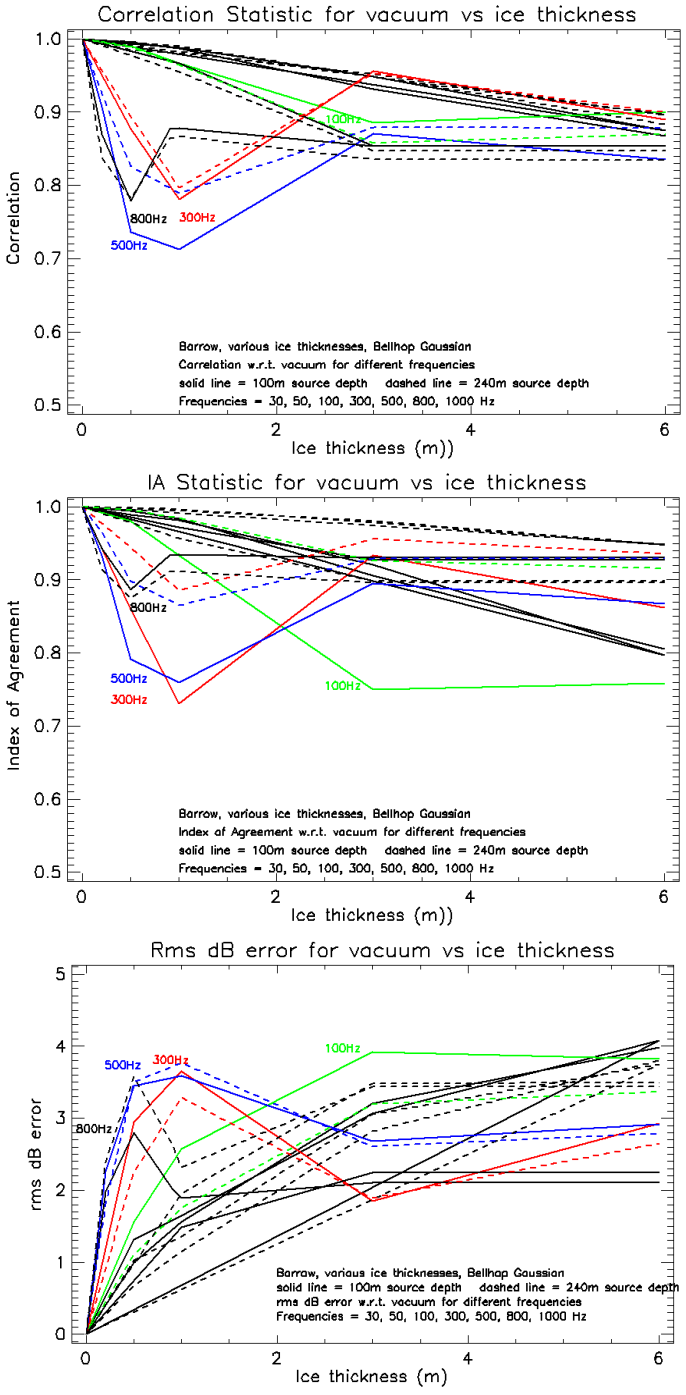

Figure 16. Barrow Strait statistics between a vacuum BC and ice of various thicknesses. The plots of 100 Hz, 300 Hz, 500 Hz and 800 Hz are identified by color and label.

Observations from these statistics

The statistics in this section are comparisons of the ice of various thicknesses vs vacuum boundary conditions using the Bellhop model. Source depths are shown as solid or dashed lines. The following observations are made:

- For ice thicknesses more than 3 m, almost all the frequencies and source depths behave in the same way, slowly declining in correlation and IA and slowly increasing in rms error as the ice thickens as compared to the vacuum boundary condition case.
- Conversely as should be expected, all frequencies and source depths approach perfect agreement with a vacuum boundary condition as the ice thins to zero.
- In the range of 0.5 to 3 m ice thickness, the four frequencies of 100, 300, 500, and 800 Hz show a resonance interaction that lowers their correlations and raises their errors.
- Note that the error of the 100 Hz signal with 3 m of ice is not equal to the error of the 300 Hz signal with 1 m of ice. That is, while the reflection coefficients of those two reciprocal cases are equal, the propagation is not.

5.2 Baffin Bay

The Baffin Bay region chosen for this study featured a flat 2200 m depth with a three-point sound speed profile [0 m,1440 m/s], [250 m,1452.5 m/s], [2200 m,1488 m/s] that produces positive upward refracting gradients. The receiver was placed at 2050 m depth. The sources were at 100 m and 2050 m.

5.2.1 Same model with different boundary conditions

Correlation and IA vs frequency, same model, different BC

Figure 17 shows the correlation as a function of frequency from 30 Hz to 1000 Hz between transmission loss from the same models under 3 m of ice with shear versus ice without shear (fluid ice) (top), a vacuum (middle) and a rigid BC (bottom) for a source depth of 100 m (solid line) and 2050 m (dashed line) and a receiver depth of 2050 m. The statistics from both models are plotted, with Prolos in red and Bellhop in black.

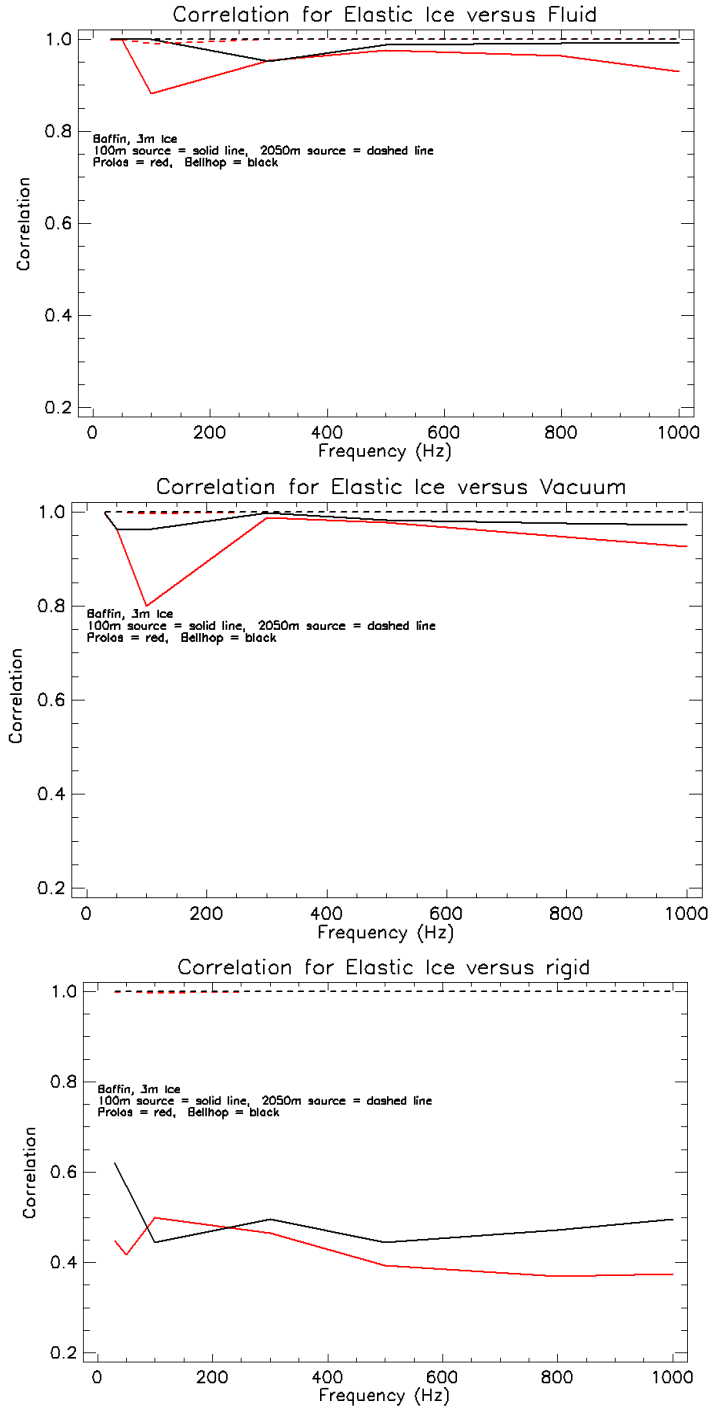

Figure 17. Impact of ice in Baffin Bay: Correlations vs frequency at 100 m (solid) and 2050 m (dashed), Prolos (red) and Bellhop (black). Top: correlation between elastic and fluid ice. Middle: correlation between elastic ice and vacuum. Bottom: correlation between elastic ice and a rigid boundary condition.

Figure 18 shows the index of agreement vs frequency for ice vs fluid (top), ice vs vacuum (middle), and for ice vs rigid (bottom) for each model at two source depths.

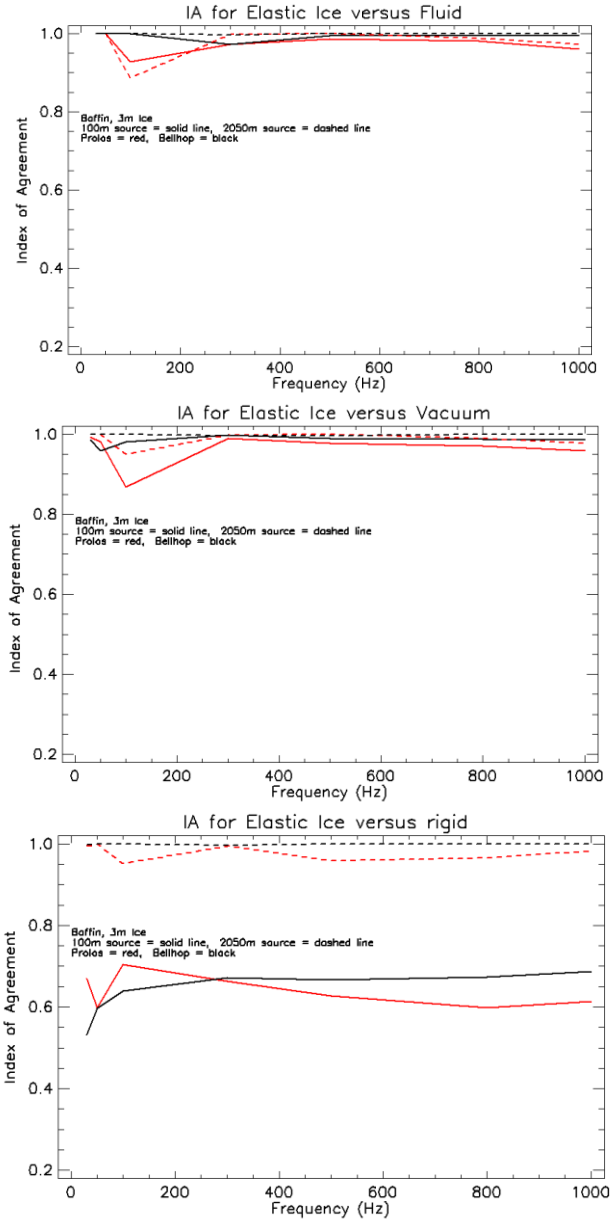

Figure 18. Impact of ice in Baffin Bay: Index of Agreement vs frequency at 100 m (solid) and 2050 m (dashed), Prolos (red) and Bellhop (black). Top: IA between elastic and fluid ice. Middle: IA between elastic ice and vacuum, Bottom: IA between elastic ice and a rigid boundary condition.

Rms dB error vs frequency, same model, different BC

Figure 19 shows the rms dB error vs frequency in Baffin Bay for ice vs fluid (top) and ice vs vacuum (middle) and ice vs a rigid BC (bottom) at two source depths for each model. Bellhop is shown in black and Prolos in red.

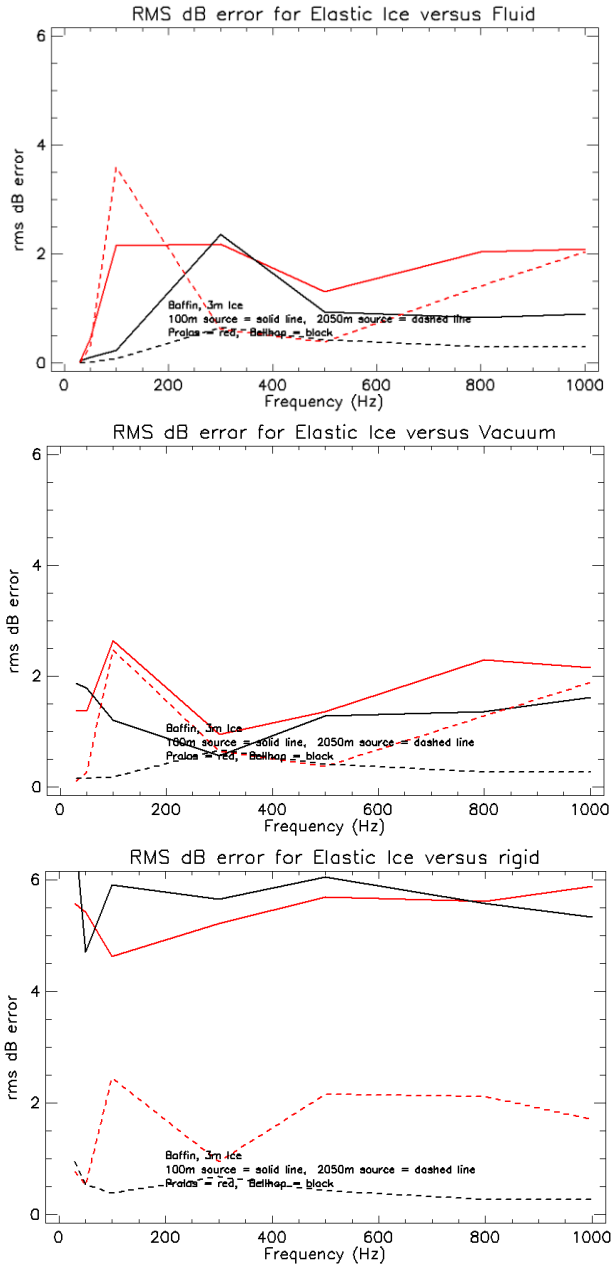

Figure 19. Impact of ice in Baffin Bay: Rms dB error vs frequency at 100 m (solid) and 2050 m (dashed), Prolos (red) and Bellhop (black). Top: Rms error between elastic and fluid ice. Middle: Rms error between elastic ice and vacuum, Bottom: Rms error between elastic ice and a rigid boundary condition.

Observations from these statistics

The statistics in this section are comparisons of the ice vs fluid, ice vs vacuum, and ice vs rigid boundary conditions using the same model in Baffin Bay. Both model statistics are shown, Bellhop is black and Prolos is red. Source depths are shown as solid or dashed lines. The following observations are made:

- Fluid ice (no shear): Both the correlation and the index of agreement statistical measures are showing the same trends and both have very high values for the fluid case at all frequencies from both models and both source depths, which leads to the conclusion that in Baffin Bay, the elastic nature of the 3 m of ice is not important and it can be treated as a fluid. The rms error also supports this conclusion, having a very low value under 2 dB in most cases.
- Vacuum (ice-free): In the comparison of ice vs vacuum, the statistics are very similar to the fluid case, which leads to the conclusion that the high-speed interface could probably be ignored altogether.
- Rigid (no penetration, no phase shift): In the comparison of ice vs rigid, the statistics are very poor for the shallow source. Correlations and IA values are much lower and the rms errors are nearly 3 times higher than those of the deep source or any of the other boundary conditions.

5.2.2 Ice thickness effects

The importance of the ice thickness in Baffin Bay was studied using Bellhop, using the Gaussian algorithm. Frequencies from 30 Hz to 1000 Hz were input for ice thicknesses varying from 0 to 6 m. Both source depths of 100 m and 2050 m were tested with the receiver at 2050 m. The statistics are plotted in Figure 20 for all frequencies and source depths, and those that show unusual behaviour are coloured and labeled.

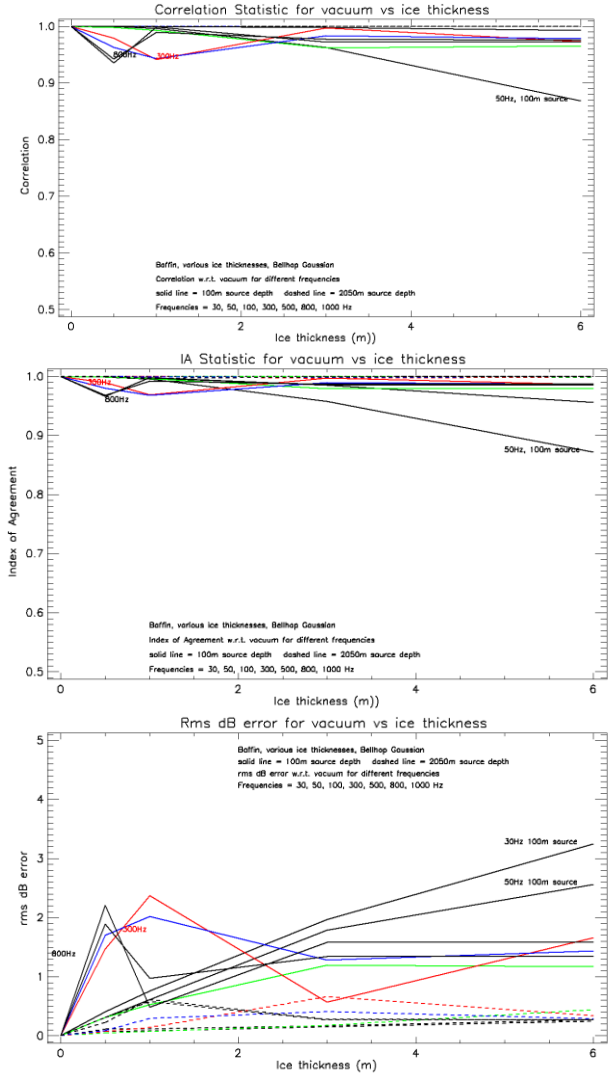

Figure 20. Baffin Bay statistics between a vacuum BC and ice of various thicknesses. Some frequencies are identified by label and color.

Observations from these statistics

The statistics in this section are comparisons of the ice of various thicknesses vs vacuum boundary conditions using the Bellhop model in the Baffin Bay region. Source depths are shown as solid or dashed lines. The following observations are made:

- Comparing these figures with those from the Barrow Strait, (Figure 16), we see that the presence of ice has a much smaller effect in the deeper waters of Baffin Bay.
- The shallow sources at 100 m are most affected by the changes in ice thickness. The deep source at 2050 m shows very little change in any of the statistics for any ice thickness.

- The resonances in the mid frequencies from the shallow source are also evident in the Baffin Bay statistics, but to a much smaller extent than was found in the Barrow Strait statistics.

This makes sense, since there are fewer boundary interactions in the deeper water.

6 MODEL-TO-MODEL COMPARISONS WITH SAME BOUNDARY CONDITIONS

In this section, each boundary condition is used in turn to compare the output from the two models, that is, each comparison is using the same boundary condition for the two models. All boundary conditions are shown on the graphs.

6.1 Barrow Strait

The Barrow Strait region chosen for this study featured a flat 250 m depth with a two point sound speed profile [0 m,1440 m/s] to [250 m,1452.5 m/s] that produces a positive upward refracting gradient of 0.05 m/s/m.

6.1.1 Same boundary conditions, different models

Correlation, index of agreement, and rms dB error, same BC, different model

Figure 21 (top) shows the correlation between Prolos and Bellhop for the boundary conditions of ice (black), fluid (red), vacuum (green) and rigid (blue) at source depths of 100 m (solid) and 240 m (dashed). Figure 21 (middle) shows the index of agreement for the same and Figure 21 (bottom) shows the rms dB error.

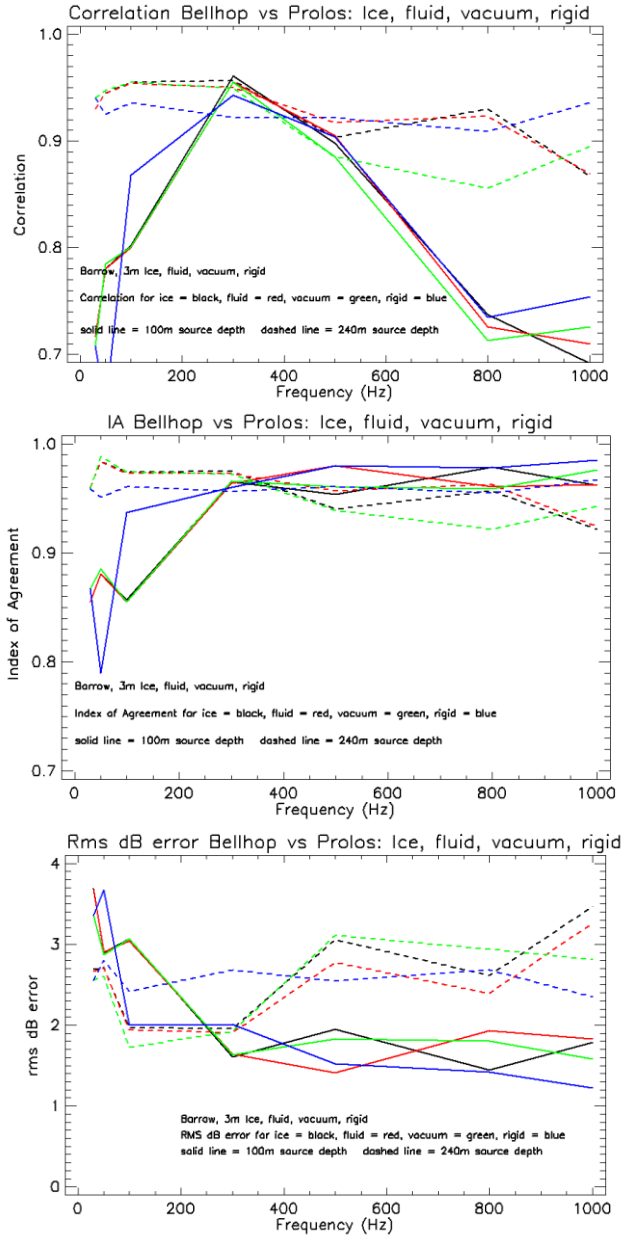

Figure 21. Model comparisons in Barrow Strait: Top: Correlation between Prolos and Bellhop under ice (black), fluid (red), vacuum (green) and rigid (blue) for sources at 100 m (solid) and 240 m (dashed). Middle: IA for same. Bottom: rms dB error for same.

Observations from these statistics

The statistics in this section show the goodness-of-fit of Bellhop and Prolos over the frequency span from 30 Hz to 1000 Hz in the Barrow Strait region using each of the different boundary conditions of ice, fluid, vacuum and rigid. The following observations are made:

- The type of boundary condition makes very little difference in the statistics. This shows that the two models are handling all the boundary conditions in the same way. And there is particularly good agreement between the models above 200 Hz for the shallow source.
- The correlation and index of agreement statistics are similar for the 240 m source depth, but the IA remains as strong over the entire frequency range while the correlation falls at the higher frequencies for the 100 m source depth. The fields are very rapidly fluctuating at the higher frequencies, and this may cause the correlation to fall due to slight misalignments. The rms error remains low at higher frequencies, indicating the two models are essentially in agreement.
- The correlation and IA both fall below 300 Hz for the 100 m source while holding steady and strong for the 240 m source. This may be because at lower frequencies, the Bellhop caustic corrections (Section 2.4.4) are playing a larger role in field formation and also when source and receiver are co-located, the direct path is at a low angle and low angles more frequently trigger the caustic corrections.
- The rms dB error rises below 300 Hz, where Bellhop underestimates the field strength because of its caustic corrections. Error levels from 300 Hz to 1000 Hz are similar, with about 1 dB less error for the 100 m source than for the 240 m source.

6.2 Baffin Bay

The Baffin Bay region chosen for this study featured a flat 2200 m depth with a three-point sound speed profile [0 m,1440 m/s], [250 m,1452.5 m/s], [2200 m,1488 m/s] that produces positive upward refracting gradients. The receiver was placed at 2050 m depth.

6.2.1 Same boundary conditions, different models

Correlation, index of agreement and rms dB error, same BC, different model

Figure 22 (top) shows the correlation between Prolos and Bellhop for the boundary conditions of ice (black), fluid (red), vacuum (green) and rigid (blue) at source depths of 100 m (solid) and 2050 m (dashed). The middle plot shows the index of agreement for the same and the bottom plot shows the rms dB error for the same.

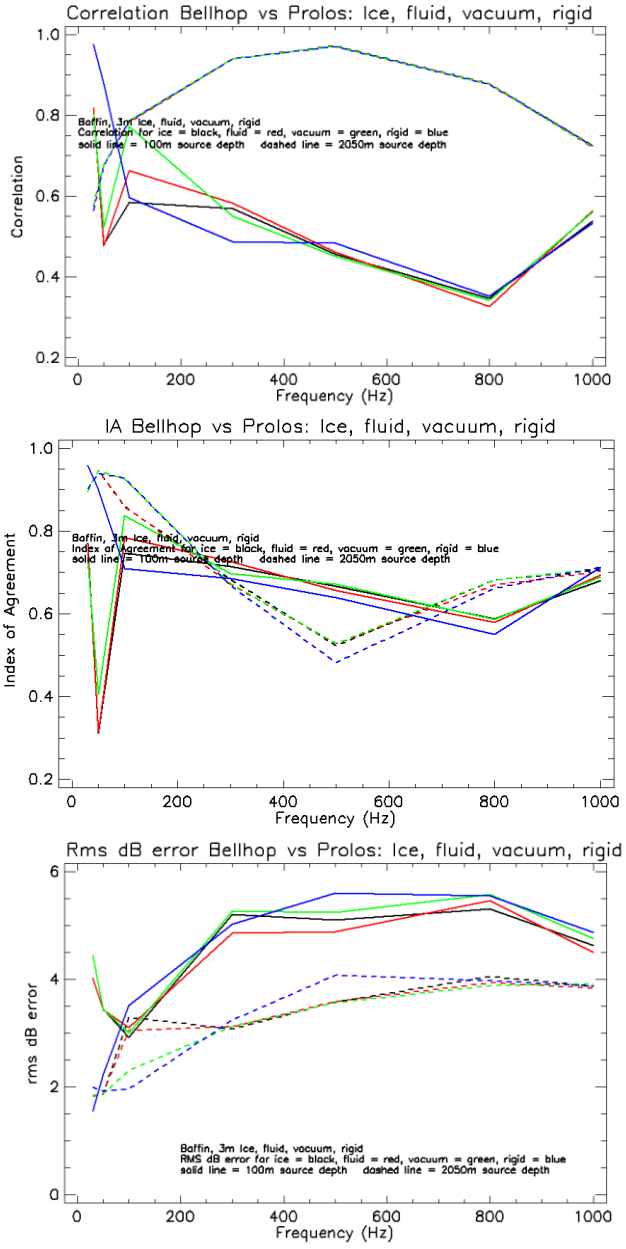

Figure 22. Model comparisons in Baffin Bay: Top: Correlation between Prolos and Bellhop under ice (black), fluid (red), vacuum (green) and rigid (blue) for sources at 100 m (solid) and 2050 m (dashed). Middle: IA for same. Bottom: rms dB error for same.

Observations from these statistics

The statistics in this section show the goodness-of-fit of Bellhop and Prolos over the frequency span from 30 Hz to 1000 Hz in the Baffin Bay region using each of the different boundary conditions of ice, fluid, vacuum and rigid. The following observations are made:

- The type of boundary condition makes very little difference in the statistics. This shows that the two models are handling all the boundary conditions in the same way, and the deeper waters of Baffin Bay are less influenced by the surface boundary conditions, particularly for the deep source.
- The correlation and index of agreement statistics do not show the same trends for the deep source, and the rms error is lower for the deep source.

7 CONCLUSIONS

7.1 Model deficiencies

Ice model:

This ice reflection model contains no scattering losses due to roughness and has no inherent range dependence. Bellhop permits the definition of a range dependent altimetry similar to its range dependent bathymetry, which can be used to portray an ice keel field. However, this study was not addressing the impact of the range dependence of the ice roughness, but instead it was to concentrate on the effects of modelling ice as an elastic media versus either a rigid or a fluid boundary. Therefore, in the implementation of this ice model, the model's inputs of ice properties and thickness were not made range dependent and the under-ice topography was assumed flat.

While the ice model can handle layers of ice of differing properties, they must all be elastic, meaning it cannot predict the effects of occluded seawater pockets.

The ice model seems to be unstable in thick ice. Figure 8 demonstrates a lot of low angle instability occurring in 10 m ice thickness at 600 Hz which is an h/λ of 1.6.

Bellhop:

A caustic correction is implemented in the Gaussian Beam algorithm of Bellhop that forces the beamwidth of the Gaussian to be no smaller than $\pi\lambda$, which in turn caps the amplitude of the pressure. For low frequencies (under 300 Hz) with long wavelengths, this limitation is often invoked, leading to underestimation of the field strength and higher transmission loss levels. Removing this caustic correction enables Bellhop to correctly match Prolos at 50 Hz, but leads to erroneous caustic spikes at higher frequencies as shown in Figure 5. The GeoHat algorithm of Bellhop has no caustic corrections and correctly matches Prolos at 50 Hz but also reveals caustic spikes at higher frequencies.

The Bellhop users guide suggests not using the model for receivers near the boundaries, because the ray method does not account for secondary ensonification from reflections. The study parameters originally called for receivers 10 m above the bottom, however the fit between Bellhop and Prolos was poor. Additional field contributions from image sources were tested and they did improve the result, but not sufficiently to satisfy the modelers. As the purpose of this study was to contrast the effects of surface boundary conditions, it was felt that the best possible agreement should be obtained under the simple pressure release surface so that changes in the boundary would be clearly defined. Therefore, the receiver was moved higher in the water

column until good agreement between the models was achieved. Contrast Figure 3 with Figure 2.

The incoherent summation of rays in Bellhop is computed in a fundamentally different way from the standard sum of magnitudes. The resulting incoherent transmission loss often shows a lot of structure and is not at all similar to the Prolos incoherent result (which is a well-defined range average of the intensity), see Figure 1. Therefore, in this study where the incoherent result is used to aid in rms dB error estimation, only the Prolos result was used.

Prolos:

The normal mode formulation in Prolos includes only the trapped modes, so modes above the critical angle of the sediment are neglected. This limitation means that for short ranges the predictions would be low because of the missing contributions from higher angle modes. For the comparisons in this paper, the first 1 km of transmission loss was omitted from the statistics to mitigate the influence of this missing energy, and Bellhop was run using rays that were mostly below the critical angle.

Prolos requires a sediment halfspace that is somewhat harder and faster than the water in order for the modes to converge without having to define a false sub-bottom layer. It was found that the sediment estimates for the silty sand found in the Barrow Strait, which in some references suggested a speed ratio of unity and a very low density ratio, were too soft to represent a basement halfspace leading to convergence problems, and therefore the sediment was defined as medium sand with a speed ratio of 1.18 and a density ratio of 1.8. This harder bottom enabled very good agreement between Bellhop and Prolos as shown in Figure 3.

The implementation of the reflection coefficient in Prolos is new, has not been thoroughly tested, and has some approximations that should be improved. The good agreement with Bellhop through the statistical tests is an indication that its predictions are reasonable, but both models should be tested against other models and benchmark cases, including those that properly treat elastic layers.

7.2 Impact of ice

In most cases, treating the ice as a fluid (no shear) or even ignoring it altogether and using a vacuum boundary condition is not a cause of major model errors. In the deeper waters of Baffin Bay with a deep receiver, the inclusion of an elastic ice boundary has almost no effect.

However, it seems that the rigid boundary condition is never a good approximation for an ice boundary. There is a phase difference that causes the correlation to fall significantly and the rms dB errors are much higher (see Figure 10 and Figures 13-15 in the Barrow Strait and Figures 17-

19 in Baffin Bay (shallow source)) This may impact current modelling treatments of ice if the modelers are using a rigid boundary condition coupled with a roughness scattering loss term as a substitute for elastic ice.

There appear to be some frequency specific (200-500 Hz region) structure in the statistical comparisons of ice with shear to the other boundary conditions, as shown in Figures 13-15. This implies that the inclusion of shear may be slightly more important in this frequency band.

The depth of ice appears to also contribute to the structure of the statistics, as shown in Figures 16 and 20, where ice thicknesses below 3 m exhibit considerable differences from a vacuum boundary condition in the mid frequency range from 300–800 Hz. For ice thicknesses above 3 m, all the statistics appear to show the same behaviour. This might imply that thin first year ice needs a more careful treatment than thick multi-year ice. These two figures also show that the impact of ice thickness is diminished in deeper water, particularly for deep sources and receivers.

7.3 Model-to-model comparisons

Model to model comparisons between Bellhop and Prolos in both Arctic regions show that the two models are in very close agreement in their predictions for all four boundary conditions tested from 30 Hz to 1000 Hz. There are no major differences in model-to-model fit caused by any of the boundary conditions.

There are however differences in the quality of agreement between Bellhop and Prolos based on the source depth. In the deeper water of Baffin Bay, the two models have a poorer correlation and higher rms dB errors for the shallower source, while in the Barrow Strait, the two models show more rms dB error for the deeper source. And in setting up the study, Bellhop was found to produce poor agreement with Prolos when the receiver was close to the boundary.

The poorer fit in Bellhop at low frequencies below 300 Hz is due to the caustic corrections that the Bellhop Gaussian beam algorithm imposes which causes an underestimation of the field strength.

The agreement between the models is good at frequencies above 300 Hz where the correlation falls somewhat because of the highly fluctuating field however the index of agreement remains high and the rms dB errors remain low.

7.4 Suggestions for future study

- Under-ice structures and range dependent properties were not considered in this study. The effects of large scale scattering and redirection of rays from ice topography may

well be much more important than the inclusion of shear in the ice. This aspect of ice interaction should be compared to the elastic contributions of the ice to rank the effects.

- In this study, it was found that Bellhop underestimated the field when close to a reflecting boundary. A good study topic could be to determine quantitatively how close is close. One might assume this restriction is based on wavelength, however, the loss characteristics of the reflection might also play a role, and the roughness of the bathymetry may also influence the proximity rule.

- The intrusion of the caustic correction in the Gaussian beam algorithm of Bellhop, found here particularly at lower frequencies in the shallow Barrow Strait region, could be studied. This might lead to an improved capping value for shallow water cases.

- The use of the ice reflection coefficient for transmission loss calculations has not been validated against a "benchmark" solution; e.g., a normal mode model that handles elastic layers. Any problem with it will appear in the predictions of both models here.

- The frequency specific structure shown in Figures 13–15, and noted in Section 7.2, warrants more attention.

8 REFERENCES

Baxley, P. A., Bucker, H., & Porter, M. (ECUA 2000). Comparison of Beam Tracing Algorithms. *Proceedings of the Fifth European Conference on Underwater Acoustics.* Lyon, France.

Ellis, D. D. (1985). *A two-ended shooting technique for calculationg normal modes in underwater sound propagation.* Darthouth, NS, Canada: Defence Research Establishment Atlantic, DREA Report 85/105.

Ellis, D. D., & Chapman, D. (1985). A simple shallow water propagation model including shear wave effects. *J. Acoust. Soc. Am. 78*, 2087-2095.

Etter, P. (2013). *Underwater Acoustic Modelling and Simulation, Fourth Edition.* Boca Raton, Florida: CRC Press, Taylor and Francis Group.

Hughes, S. J., Ellis, D., Chapman, D., & Staal, P. (1990). Low-frequency acoustic propagation loss in shallow water over hard-rock seabeds covered by a thin layer of elastic-solid sediment. *J. Acoust. Soc. Am., 88*, 283-297.

Jensen, F., Kuperman, W., Porter, M., & Schmidt, H. (2011). *Computational Ocean Acoustics* (2nd ed.). Springer.

McCammon, D. F., & Ellis, D. (2015). *Addition of Beam Displacement to Gaussian Beam Model.* Maritime Way Scientific Contractor Report.

McCammon, D., & McDaniel, S. (1985). The influence of the physical properties of ice on reflectivity. *J. Acoust. Soc. Am., 77(2)*, 499-507.

Ocean Acoustics Library. (last accessioned June 1, 2017). Retrieved from http://oalib.hlsresearch.com/

Ogilvy, J. A. (1991). *Theory of Wave Scattering from Random Surfaces.* New York: Adam Hilger.

Porter, M. (2010). *The BELLHOP Manual and User's Guide: Preliminary draft.* La Jolla, CA: Heat, Light and Sound Research, Inc.

Statistics. (last accessioned June 1, 2017). Retrieved from http://cirpwiki.info/wiki/Statistics

Tindle, C., & Weston, D. (1980). Connection of acoustic beam displacement, cycle distances, and attenuations for rays and normal modes. *J. Acoust. Soc. Am. 67*, 1611-1622.

Willmott, C., Ackleson, S., Davis, R., Feddema, J., Klink, K., Legates, D., . . . Rowe, C. (1985). Statistics for the evaluation and comparison of models. *Journal of Geophysical Research 90 (C5)*, 8995-9005.

9 APPENDIX A. IMPLEMENTING THE ICE BOUNDARY CONDITION IN PROLOS

The Prolos model (Ellis, 1985) is applicable to an environment having fluid layers, with a pressure release boundary at the surface and a halfspace at the bottom. It is possible to extend the normal mode formulation to handle elastic layers (Hughes, Ellis, Chapman, & Staal, 1990), but the procedure is fairly complicated and subject to numerical issues. A simpler formulation for water over a bottom shear layer was available (Ellis & Chapman, 1985), and a quick attempt was made to adapt it to an ice layer at the surface. However, things did not work immediately, and it applied only for a single homogeneous ice layer, so that approach was shelved in favour of an arbitrary reflection coefficient at the ocean surface.

The mode boundary condition can be obtained from the phase of the reflection coefficient, and the mode attenuation coefficient obtained from the reflection loss and cycle distance (Tindle & Weston, 1980). Tindle and Weston [Eq. (11)] showed that the normal mode boundary condition could be obtained from the bottom reflection coefficient

$$\phi = 2\tan\left\{\frac{Z_1'(h)}{[\gamma_1(h)Z_1(h)]}\right\}, \tag{A0}$$

where $Z_1(z)$ is the normal mode pressure for mode u_n in the water, $\gamma_1(z)$ is the vertical wavenumber in the water and h is the depth of the interface.

The usual normal mode boundary condition at the ocean surface is $u_n(z) = 0$, corresponding to a pressure release surface, $R = -1$. In general, $R = |R|e^{i\phi}$ (for pressure release, $\phi = \pm\pi$, where the ± depends on convention).

The mode depth function can be written as $u_n(z) = A_n(z)\sin\psi(z)$, where $A_n(z)$ is relatively slowly varying, $\psi(z)$is monotonically increasing, and at the bottom boundary $(n - \frac{1}{2})\pi < \psi(z) < n\pi$. In the WKB-like approach used in Prolos, $A_n(z) = \sqrt{u_n(z)^2 + [u_n'(z)/\gamma_{1n}(z)]^2}$ and $\psi(z) = \psi_0 + \int_0^z \gamma_{1n}(z')dz'$. With the pressure release boundary, $\psi_0 = 0$, but with a reflection coefficient $|R|e^{i\phi}$, then $\psi_0 = \frac{\pi+\phi}{2}$, where our convention is that $\phi = -\pi$ at grazing angle of zero.

Since Prolos uses isospeed layers, the starting condition in the first water layer is

$$\frac{u_n(z)}{u_n'(z)} = \gamma_{1n}^{-1}\tan\psi_0. \tag{A2}$$

The mode attenuation can be obtained from

$$\delta_n = \frac{1-|R|}{D_n}, \tag{A3}$$

where the reflection coefficient R is evaluated at the angle incident on the interface. D_n is the mode cycle distance, for large mode numbers given by

$$D_n = -2\pi/(dk_n/dn) \approx 4\pi/(k_{n-1} - k_{n+1}) , \tag{A4}$$

where the wavenumber is k_n. In the first equality n is considered as continuous, and the second approximation is a numerical evaluation.

An expression for the cycle distance using only mode n can be obtained from (Tindle & Weston, 1980)[Eq. (25)]

$$D_n = 4\gamma_{1n}(z)k_n /\{[\gamma_{1n}(z)\, u_n(z)]^2 + [u_n'(z)]^2\}, \tag{A5}$$

as long as terms involving the derivative $\gamma_{1n}'(z)$ are negligible. This will be exactly true at the sound speed minimum, and a good approximation (an "invariant") at any depth away from turning points. There is a slight error in the mode normalization with this approach, since it ignores contributions in the ice layer. It could be corrected (Tindle & Weston, 1980)[Eq. (32)] by getting the cycle distance from the wave number differences, but (being small for an ice layer) is not corrected for the calculations in this paper.

DOCUMENT CONTROL DATA

*Security markings for the title, authors, abstract and keywords must be entered when the document is sensitive

1. ORIGINATOR (Name and address of the organization preparing the document. A DRDC Centre sponsoring a contractor's report, or tasking agency, is entered in Section 8.)

Maritime Way Scientific Ltd
1420 Youville Drive, Unit 5A
Ottawa ON K1C 7B3

2a. SECURITY MARKING (Overall security marking of the document including special supplemental markings if applicable.)

CAN UNCLASSIFIED

2b. CONTROLLED GOODS

NON-CONTROLLED GOODS
DMC A

3. TITLE (The document title and sub-title as indicated on the title page.)

Model-to-model comparison of low-frequency acoustic models for Arctic environments: Impact of Ice

4. AUTHORS (Last name, followed by initials – ranks, titles, etc., not to be used)

McCammon, D.; Ellis, D.

5. DATE OF PUBLICATION (Month and year of publication of document.)	6a. NO. OF PAGES (Total pages, including Annexes, excluding DCD, covering and verso pages.)	6b. NO. OF REFS (Total references cited.)
April 2018	54	14

7. DOCUMENT CATEGORY (e.g., Scientific Report, Contract Report, Scientific Letter.)

Contract Report

8. SPONSORING CENTRE (The name and address of the department project office or laboratory sponsoring the research and development.)

DRDC - Atlantic Research Centre
Defence Research and Development Canada
9 Grove Street
P.O. Box 1012
Dartmouth, Nova Scotia B2Y 3Z7
Canada

9a. PROJECT OR GRANT NO. (If appropriate, the applicable research and development project or grant number under which the document was written. Please specify whether project or grant.)	9b. CONTRACT NO. (If appropriate, the applicable number under which the document was written.)
	W7707-145690 Call-up # 11

10a. DRDC PUBLICATION NUMBER (The official document number by which the document is identified by the originating activity. This number must be unique to this document.)	10b. OTHER DOCUMENT NO(s). (Any other numbers which may be assigned this document either by the originator or by the sponsor.)
DRDC-RDDC-2018-C079	

11a. FUTURE DISTRIBUTION WITHIN CANADA (Approval for further dissemination of the document. Security classification must also be considered.)

Public release

11b. FUTURE DISTRIBUTION OUTSIDE CANADA (Approval for further dissemination of the document. Security classification must also be considered.)

12. KEYWORDS, DESCRIPTORS or IDENTIFIERS (Use semi-colon as a delimiter.)
acoustic modelling; Arctic acoustics
13. ABSTRACT/RÉSUMÉ (When available in the document, the French version of the abstract must be included here.)